JGR Atmospheres

RESEARCH ARTICLE
10.1029/2021JD035062

New Estimation of the NO_x Snow-Source on the Antarctic Plateau

A. Barbero[1], J. Savarino[1], R. Grilli[1], C. Blouzon[1], G. Picard[1], M. M. Frey[2], Y. Huang[3], and N. Caillon[1]

[1]Grenoble INP (Institute of Engineering), IGE, University of Grenoble Alpes, CNRS, IRD, Grenoble, France, [2]British Antarctic Survey, Natural Environment Research Council, Cambridge, UK, [3]Department of Civil and Environmental Engineering, Wayne State University, Detroit, MI, USA

Key Points:

- Photolabile nitrate in snow behaves as a single-family source with common photochemical properties
- New quantification of snow-nitrate photolysis using flux chamber experiments
- NO_x snow-source could be better defined and differences in photolytic mechanics of Antarctica's different regions could be addressed

Correspondence to:

A. Barbero,
albane.barbero@univ-grenoble-alpes.fr

Citation:

Barbero, A., Savarino, J., Grilli, R., Blouzon, C., Picard, G., Frey, M. M., et al. (2021). New estimation of the NO_x snow-source on the Antarctic Plateau. *Journal of Geophysical Research: Atmospheres*, *126*, e2021JD035062. https://doi.org/10.1029/2021JD035062

Received 13 APR 2021
Accepted 3 SEP 2021

Author Contributions:

Conceptualization: A. Barbero, J. Savarino
Data curation: A. Barbero
Formal analysis: A. Barbero, G. Picard
Funding acquisition: J. Savarino, R. Grilli
Investigation: A. Barbero, J. Savarino, R. Grilli, C. Blouzon, G. Picard, M. M. Frey, Y. Huang
Methodology: A. Barbero, J. Savarino, R. Grilli, C. Blouzon, G. Picard, M. M. Frey, Y. Huang
Resources: J. Savarino, R. Grilli, C. Blouzon, G. Picard, N. Caillon
Supervision: J. Savarino, R. Grilli
Validation: A. Barbero, J. Savarino, R. Grilli, M. M. Frey, N. Caillon
Writing – original draft: A. Barbero
Writing – review & editing: A. Barbero, J. Savarino, R. Grilli, G. Picard, M. M. Frey, Y. Huang

Abstract To fully decipher the role of nitrate photolysis on the atmospheric oxidative capacity in snow-covered regions, NO_x flux must be determined with more precision than existing estimates. Here, we introduce a method based on dynamic flux chamber measurements for evaluating the NO_x production by photolysis of snowpack nitrate in Antarctica. Flux chamber experiments were conducted for the first time in Antarctica, at the French-Italian station Concordia, Dome C (75°06'S, 123°20'E, 3233 m a.s.l) during the 2019–2020 summer campaign. Measurements were gathered with several snow samples of different ages ranging from newly formed drifted snow to 6-year-old firn. Contrary to existing literature expectations, the daily average photolysis rate coefficient, $\overline{J_{NO_3^-}}$, did not significantly vary between differently aged snow samples, suggesting that the photolabile nitrate in snow behaves as a single-family source with common photochemical properties, where a $\overline{J_{NO_3^-}} = (2.37 \pm 0.35) \times 10^{-8}\ s^{-1}$ (1σ) has been calculated from December 10th 2019 to January 7th 2020. At Dome C summer daily average NO_x flux, F_{NO_x}, based on measured NO_x production rates was estimated to be $(4.3 \pm 1.2) \times 10^8$ molecules $cm^{-2}\ s^{-1}$, which is 1.5–7 times less than the net NO_x flux observed previously above snow at Dome C using the gradient flux method. Using these results, we extrapolated an annual continental snow sourced NO_x budget of 0.017 ± 0.003 Tg·N y^{-1}, ~2 times the nitrogen budget, (N-budget), of the stratospheric denitrification previously estimated for Antarctica. These quantifications of nitrate photolysis using flux chamber experiments provide a roadmap toward a new parameterization of the $\sigma_{NO_3^-}(\lambda, T)\phi(T, pH)$ product that can improve future global and regional models of atmospheric chemistry.

1. Introduction

The southern high-latitude regions of Antarctica are ideal for studying the connections between climate and atmospheric chemistry due to the continent's distinct geographic advantages. Antarctica's great distance from major sources of pollution, the outflow of low-level katabatic winds, and the insulating nature of the predominant atmospheric circulation combine to maintain a relative cleanliness of the Antarctic Plateau atmosphere (Savitskiy & Lessing, 1979). Therefore, Antarctica offers a continental sized natural laboratory with relatively limited direct human influences on biogeochemical cycles.

Snow-air-radiation interactions and their link to the specific oxidizing character of the polar atmosphere is key to correctly deciphering the past environmental information preserved in the ice and to understanding the present chemical stability of the Antarctic atmosphere. Previous studies suggest that a highly reactive lower atmosphere exists above the snowpack (Domine & Shepson, 2002; Grannas et al., 2007), and this raises questions about how the basic air composition within the polar atmosphere is being altered. Unexpectedly high levels of oxidants have been discovered in the continental interior as well as in the coastal regions, with atmospheric hydroxyl radical (OH) concentrations up to 4×10^6 cm^{-3} (Davis et al., 2008; Grilli et al., 2013; Kukui et al., 2014; R. L. Mauldin et al., 2001; R. Mauldin et al., 2004, 2010; Wang et al., 2007). These levels make the summer Antarctic boundary layer as oxidative as urban atmospheres, which was not expected for an atmosphere thought to have the most pristine boundary layer on Earth (Berresheim & Eisele, 1998; Davis et al., 2004). It is now well established that such high reactivity of the summer Antarctic boundary layer results, in part, from the emissions of nitrogen oxides ($NO_x \equiv NO + NO_2$) produced during photochemical release of nitrogen species from the snowpack (Honrath et al., 1999, 2000; Jones et al., 2000, 2001).

Despite the numerous observations collected at various sites during previous campaigns such as ISCAT 1998, ISCAT 2000, ANTCI and OPALE (Davis et al., 2008; R. L. Mauldin et al., 2001; R. Mauldin et al., 2004; Preunkert et al., 2012; Wang et al., 2007), using the flux gradient method with very detailed NO_x and HONO flux measurements above the snow, questions remains about how to best parameterize the snowpack source in models. Indeed, the NO_x production rate, P_{NO_x} [molecules s^{-1}] and estimated NO_x fluxes, F_{NO_x} [molecules cm^{-2} s^{-1}] above the snow are difficult to constrain, largely because of the poorly constrained quantum yield of NO_3^- photolysis in snow (Chan et al., 2018). Therefore, a robust quantification of the NO_x sources on a continental scale over Antarctica is still lacking (Frey et al., 2013, 2015; Legrand et al., 2014; Savarino et al., 2016). The chemical reactivity of the snowpack and its connection to the overlying atmosphere need further study to fully understand their linkage to snow chemical composition. Previous works have proposed different mechanisms to explain the nitrate photolysis behavior in ice and snow (e.g., Blaszczak-Boxe and Saiz-Lopez (2018) and references therein).

Chu and Anastasio (2003) suggested that the nitrate photolysis on ice is occurring in a "quasi-liquid layer" rather than in the bulk ice with a quantum yield $\phi = 0.003$ molecules $photon^{-1}$. Zhu et al. (2010) found very high values of NO_3^- quantum yield from the photolysis of HNO_3 on ice films at 308 nm and 253 K: $\phi = 0.60 \pm 0.34$ molecules $photon^{-1}$ (2σ) with the error representing the experimental scatter. Thomas et al. (2011); Thomas et al. (2012) used this simplified representation of the liquid-like layer and its chemistry to represent the complex processes occurring in the Greenland snowpack. Davis et al. (2008), developed a theory driven by two photochemical domains affecting the nitrate photo-dissociation, namely the photo-labile (with nitrate adsorbed at the snow grain surface) and buried domains. Davis et al. (2008) also proposed that surface adsorption becomes more efficient with decreasing temperatures. M. C. Zatko et al. (2013) followed Davis et al. (2008) by assuming that the NO_3^- incorporated in the snowpack by wet deposition is ingrained in the snow crystal compared to dry NO_3^- deposition, where it stays at the surface of the snow-grain, therefore more likely to dissociate into NO_x after encountering a photon, and diffuse to the surface. Meusinger et al. (2014) followed Davis et al. (2008) to decipher the quantum yield of nitrate photolysis and described the micro-physical properties of the region around the nitrate chromophore affecting its dissociation. The nitrate contained in the photo-labile domain is consumed first, being more available than the buried nitrate, hindered by a cage effect. The derived apparent quantum yields for both nitrate family were very different: $\phi^*_{buried} = 0.05$ molecules $photon^{-1}$ and $\phi^*_{photo-labile} = 0.26$ molecules $photon^{-1}$.

Bock et al. (2016) developed a nitrate air-snow exchange model and tested it against the summer observations at Dome C, which demonstrated that co-condensation, that is, the simultaneous condensation of water vapor and trace gases at the air-ice interface, was the most important process to explain nitrate incorporation in snow. Bock et al.'S (2016) model works well at cold sites on the Antarctic Plateau, where air temperatures are well below freezing and in fact below the eutectic point year-round, and where no snow melt occurs. However, the model does not reproduce the summer observations at the coast, where the temperature, relative humidity and concentration of aerosol in air and snow are much higher than that on the Plateau, and where snow surface melt is possible, strengthening previous theory of several photolytic domains aforementioned. Nonetheless, Chan et al. (2018) developed a new model and concluded that winter air-snow interactions of nitrate between the air and skin layer snow can be described as a combination of non-equilibrium surface adsorption and co-condensation on ice, coupled with solid-state diffusion inside the grain, similar to Bock et al. (2016). In addition, Chan et al. (2018) were able for the first time to reproduce the summer observations on the Antarctic Plateau and at the Coast, concluding that it is the equilibrium solvation into liquid micro-pockets, based on Henry's solubility law, that dominates the exchange of nitrate between air and snow at warmer sites, that is, where the temperatures are above the eutectic temperature.

To date, no consensus can be found in the literature about the different forms of nitrate that would allow us to reduce the modeled F_{NO_x} uncertainties. Models usually use the quantum yield of 0.003 molecules $photon^{-1}$ found by Chu and Anastasio (2003), therefore often under-predict the observations, for example, at night time at Dome C (Frey et al., 2013). A better parameterization of nitrate photolysis quantum yield as a function of snow micro-physical properties and nitrate form (ion or HNO_3 molecule) is needed to improve the models.

A major difficulty encountered for estimating F_{NO_x} is that it depends upon two components: transport (both inward and outward to the snowpack) and photochemical production/loss. Previous field studies did not

separate these two phenomena, and it was argued that transport could be neglected because the photochemical lifetime is only a few minutes while the time-scale needed for substantial transport above the snowpack is on the order of a few hours. The difficulty in measuring NO_x fluxes is due to the rather weak NO_x gradient in the atmosphere with respect to the relatively high measurement uncertainties, the measurement itself being disturbed by re-deposition of nitrate, convection and ventilation. Here, to circumvent this challenge, we present measurements of P_{NO_x} [molecules s^{-1}] under controlled flux, further converted into area flux F_{NO_x} [molecules cm^{-2} s^{-1}] to allow: i) comparison with above-snow measurements as first approximation; and ii) new leads or suggestions for atmospheric models.

The net flux above the snow surface has been previously estimated using the flux-gradient method (Frey et al., 2013): Fick's law describes how concentration gradient, $\frac{\partial c}{\partial z}$, and diffusion coefficient, K_c, of a chemical tracer relate to the diffusive flux, F: $F = -K_c \frac{\partial c}{\partial z}$ (Lenschow, 1995). However, potential impacts of photochemical transformation during transport in the open pore space of the snowpack and above may reflect on the flux estimate. Photochemical production rates, P_{NO_x} [molecules s^{-1}], can also be measured directly using dynamic flux chambers (FC). Cotter et al. (2003) were the first to measure NO_x production rates using a laboratory FC experiment, varying temperature and UV irradiation, to determine the mechanism involved in NO_x release from snow. These experiments did not exactly represent the Antarctic snowpack behavior because: i) the physical properties of the snow sample had most likely changed significantly during storage due to snow metamorphism and ii) the UV lamp used was much stronger than natural light conditions. This motivated us to conduct FC experiments on the Antarctic plateau, at Dome C, during the 2019–2020 campaign.

Flux chambers are the most widely used equipment to quantify gaseous emissions from solid or liquid surface sources (Besnard & Pokryszka, 2005; Cotel et al., 2015; Pokryszka & Tauziède, 1999; Verginelli et al., 2018), and they are widely used nowadays to assess emissions of pollutants into the atmosphere from the surface (Scheutz et al., 2008; Sihota et al., 2010; Tillman et al., 2003). A dynamic FC method developed to measure production rates from hazardous waste sites employs an inert gas that is continuously introduced at a controlled rate while an equivalent amount of gas is allowed to leave the chamber (Eklund, 1992). In our Antarctic experiments, we adapted this method for NO_x monitoring, using an open circuit FC with clean air injected and $NO_{x-bearing}$ air at the outlet of the chamber analyzed, similar to Cotter et al. (2003) laboratory FC experiment.

Our study was novel in that it directly measured photochemical production rates as close as possible to the natural system. Such experiments allow us to measure an integrated parameter: $\overline{J_{NO_3^-}}$, the daily nitrate photolysis rate coefficient. In Section 2, we provide details of the experimental studies undertaken. In Section 3, we describe the data validation process applied. In Section 4, we present the results and their analysis to evaluate the impact of this method on the NO_x production from the snowpack at Dome C and provide a rough continental extrapolation. Finally, in Section 5, we provide conclusions.

2. Method

2.1. Site Description

The FC experiments were conducted from December 10^{th} to January 7^{th} at the French-Italian station Concordia, Dome C (75°06'S, 123°20'E, 3,233 m a.s.l) during the 2019–2020 campaign. At this latitude, the station experiences polar night during the austral winter as the sun remains below the horizon from May to August. In summer (November to January) the solar zenith angle (SZA) does not go above 52° (i.e., lower than 38° above the horizon).The annual climate at Dome C is mainly cold and dry ($T_{mean} = -53 \pm 14$ °C and surface mass balance SMB = 26 kg m^{-2} yr^{-1}), typically with clear skies or elevated cirrus clouds (Palchetti et al., 2015), light winds ($W_{speed-mean} = 3.3 \pm 2.1$ m s^{-1}) and mean atmospheric pressure of $P_{mean} = 641 \pm 27$ hPa, as shown in Figure 1a.

These conditions are due to a dry and cold boundary-layer flow predominantly originating from the south ($W_{dir-mean} = 172 \pm 90°$), depicted in Figure 1b, as well as being on a dome of high altitude with an albedo close to 1. Summer is warmer and more humid than the annual mean, and the conditions encountered during the 2019–2020 FC experiments were typical of the summer climatology observed at Dome C: $T_{mean} = -29 \pm$

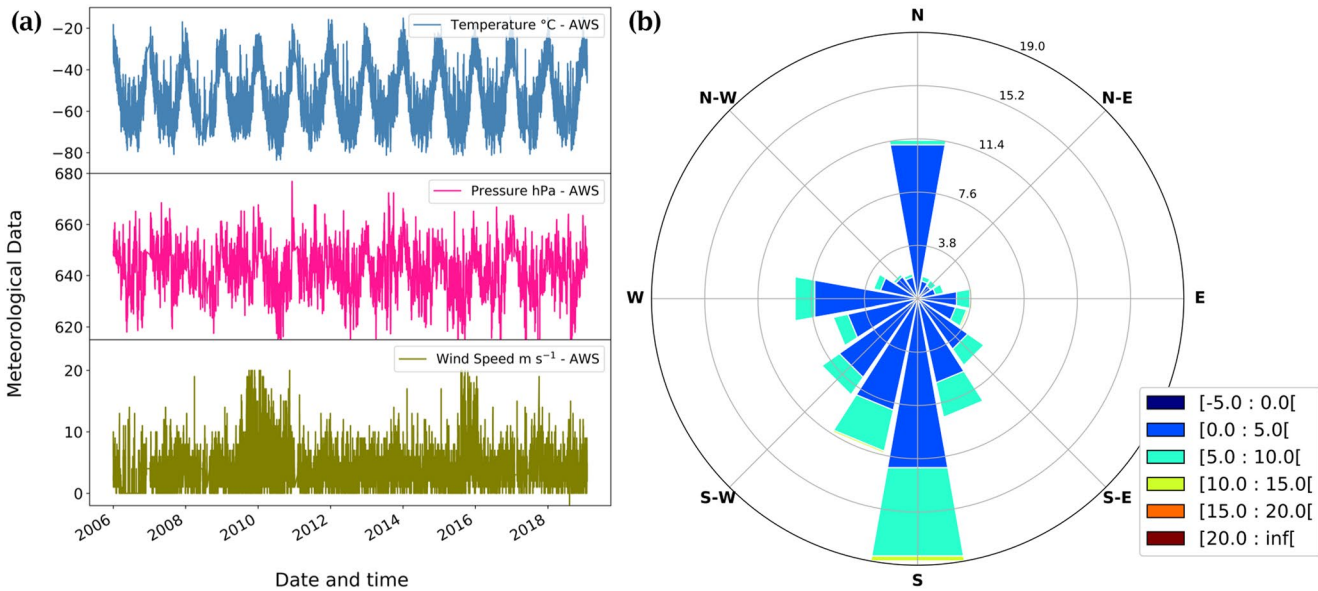

Figure 1. (a) Multiyear meteorological observations 2-m records at Dome C, Concordia station, Antarctica measured by the local automatic weather station (AWS-Vaisala Milos 520) and (b) the corresponding wind rose in m s^{-1} during the period of 2006–2019.

5°C; $P_{mean} = 655 \pm 3$ hPa; $W_{speed-mean} = 3.1 \pm 1.5$ m s^{-1} and $W_{dir-mean} = 173 \pm 80°$. More information about the meteorological conditions encountered during the experiments can be found in Appendix A.

2.2. Experiment Location and Setup

The experiment was located in the station's clean area sector, about 1 km south-west and upwind of the main station buildings (red cross in Figure 2) in a zone less subjected to pollution linked to activities taking place at Concordia since 1997. A container buried under the snow and maintained at 8 C was used to host the measuring instruments and all the equipment necessary for the experiments. The FC experiments were designed in order to study different types of snow while working as close as possible to natural conditions (natural snow, radiation, temperature, and actinic flux). By controlling the transport component of the NO_x, their production can be estimated through Equation 1:

$$P_{NO_x} = J_{NO_3^-} \times N_{NO_3^-} \quad (1)$$

where P_{NO_x} is the NO_x production in molecules s^{-1}; $J_{NO_3^-}$ is the photolysis rate constant of the snowpack nitrate in s^{-1} and $N_{NO_3^-}$ is the amount of nitrate contained in the snow expressed in molecules. Therefore, the objective was to study the NO_x production from different snows, that is, varying $N_{NO_3^-}$, and the associated diurnal cycles, that is, varying $J_{NO_3^-}$. $J_{NO_3^-}$ depends on several parameters following Equation 2:

$$J_{NO_3^-} = \int_{(\theta,\psi,\lambda)} \sigma_{NO_3^-}(\lambda,T)\phi(\lambda,T,pH)I_{act}(\theta,\psi,\lambda,z)d\theta d\psi d\lambda \quad (2)$$

where θ is the SZA; ψ marks the sun declination; λ [nm] is the wavelength; and z [m] is the snowpack's depth; $\sigma_{NO_3^-}(\lambda,T)$ is the absorption cross-section of nitrate; $\phi(\lambda,T,pH)$ and $I_{act}(\theta,\psi,\lambda,z)$ are nitrate photolysis quantum yield and actinic flux, respectively. Although the nitrate photolysis reactions (R1 to R5) produce both NO and NO_2 in the gas phase (Bartels-Rausch & Donaldson, 2006; Grannas et al., 2007), it is more relevant to directly referred to NO_x. To that end, this study focuses on the sum of NO + $NO_2 \equiv NO_x$.

$$NO_3^- \xrightarrow{h\nu} NO_2(g) + O^- \quad (R1)$$

$$NO_3^- \xrightarrow{h\nu} NO_2^- + O(^3P) \xrightarrow{H^+} HONO(g) \xrightarrow{h\nu} NO(g) + OH \quad (R2)$$

$$NO_2^- \xrightarrow{h\nu} NO(g) + O^- \quad (R3)$$

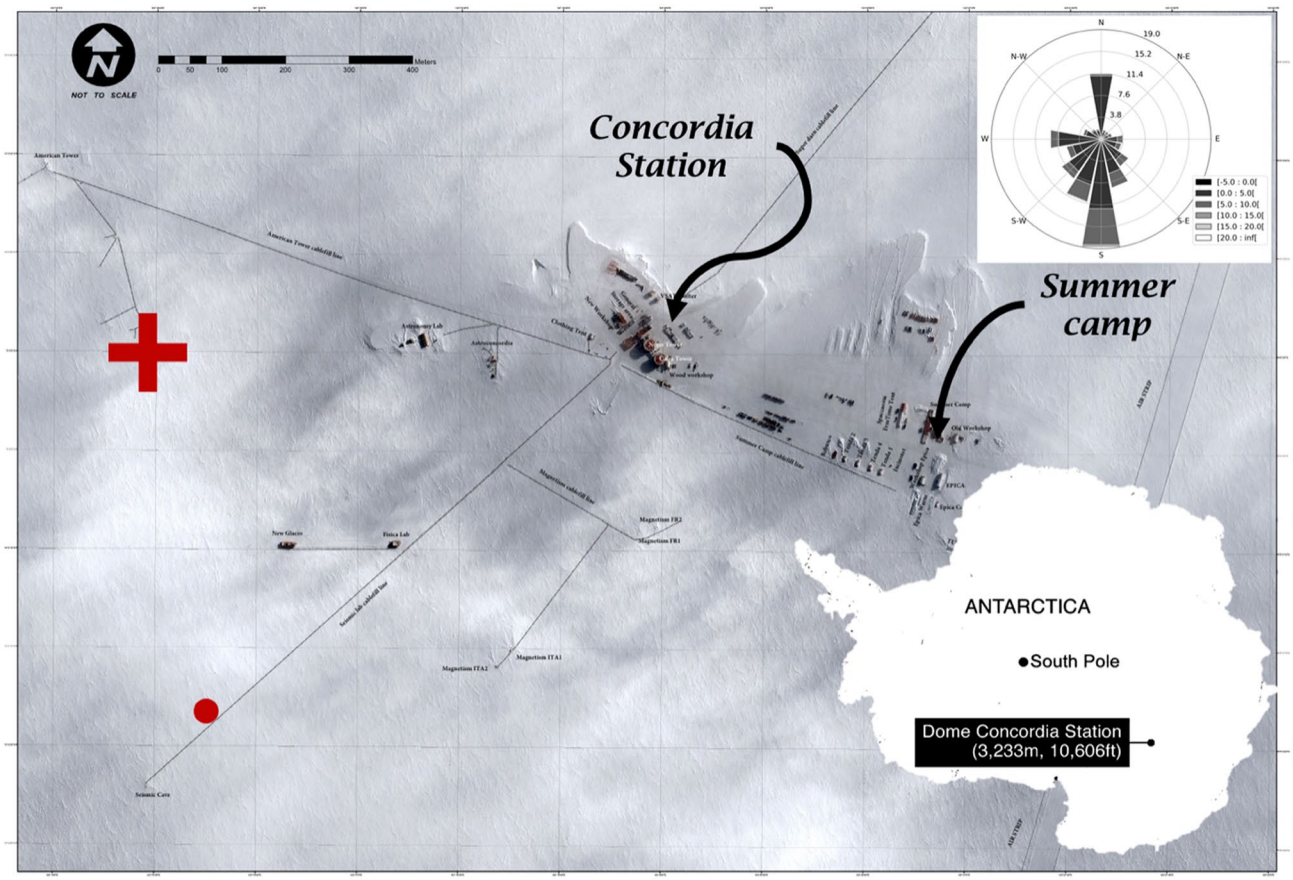

Figure 2. Aerial view of the station: the red cross marks the position of the experiments and the red dot the location of the automatic weather station (AWS-Vaisala Milos 520). The dominant wind rose is shown in the upper right-hand corner. The location of Concordia station is shown in the lower right-hand corner (*Pléiade Satellite Image—Concordia Station, Antarctica* @ CNES 2016, *Distribution Airbus DS)*.

$$O^- + H_2O \rightarrow OH^- + OH \quad \text{(R4)}$$

$$NO_2^- + OH \rightarrow NO_2(g) + OH^- \quad \text{(R5)}$$

Because photolysis of nitrate in snow occurs under UV radiation ($\lambda > 300$ nm with 305 nm the optimal wavelentgh), UV-transparent chambers are essential for the experiment. The most UV-transparent material after glass is polymethyl methacrylate (PMMA). It is lighter than glass and therefore more practical to use in the field; however, it gets very brittle in cold environment. Several PMMA materials were tested to find the best compromise between thickness and UV transparency. We found that a thickness of 8 mm offered general robustness and cold resistance while keeping the weight of an empty chamber reasonable for handling in the field (~5 kg). Within the different PMMAs, the Plexiglas Clear GS2458 GT (EBLA-GmbH Kunststofftechnik) provided the best transparency in the UV: >71% of transmitted light for λ >305 nm (transmission spectra provided in Appendix B). The chamber dimensions (70 × 21 × 21 cm) give a volume of V_{FC} ~ 0.03 m^3 and a total surface area of S_{FC} ~ 0.62 m^2, providing enough NO_x production to be detected by the monitoring instruments.

Because light attenuates quickly with depth in the snowpack following an exponential decrease, this makes the first few centimeters of the snow column dominate the availability of photons for photochemical reactions in the UV (Brandt & Warren, 1993; Domine et al., 2008; Simpson et al., 2002). At Dome C, the radiative transfer model developed by Libois et al. (2013, 2014) predicts a 95% loss of light in the snowpack after 50 cm depth at λ >305 nm (e.g., the actinic flux is effectively null below 50 cm). This defines the photic zone (Erbland et al., 2013) of 3 times the *e*-folding depths, and the model therefore assumes a mean *e*-folding depth of 17 cm, which is consistent with France et al. (2011) observations of ~10 cm for windpack layer and

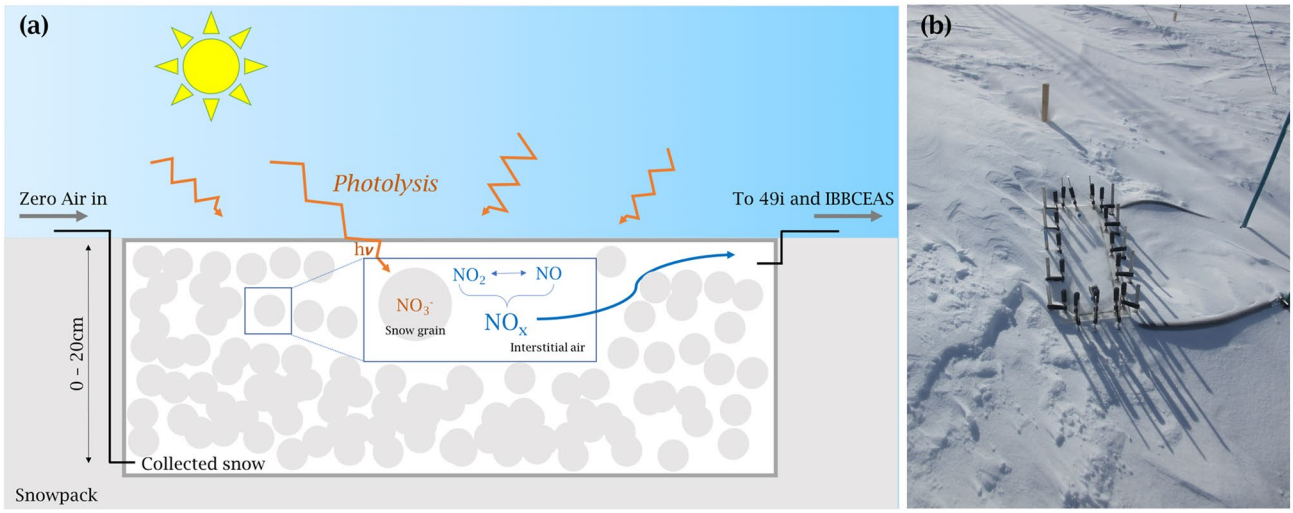

Figure 3. (a) Schematic and (b) picture of one FC experiment in the field. Note that more detailed schematic of the experiment is given in Appendix C.

~20 cm for hoar-like layer at 400 nm. We chose a chamber depth that covered one *e*-folding depth for all our snow samples, representing ~63% of NO_x produced in the snow column.

The chamber was filled with the desired snow and closed with clamps, allowing the snow to be changed and weighed easily. It was then connected to a zero-air flow at the inlet and to the analysis instruments at the outlet using $\frac{1}{4}$ (~ 0.64 cm) diameter Teflon® tubing and connectors.

The sample inlet and outlet tubes were protected from solar radiation and kept 2 to 3 C above ambient temperature to avoid any condensation occurring inside the lines. The chamber was then buried in the snow, with the upper cover at the same height as the snowpack surface, to ensure the most natural experimental conditions (Figure 3).

The zero-air flow was produced by pumping outdoor air through two serial zero-air cartridges connected in series (TEKRAN, 90-25,360-00 Analyzer Zero Air Filter) and pushed into the FC at $F_{air} = 58 \pm 17$ cm^3 s^{-1} (3.50 ± 1.05 slpm, standard liters per minute).

Only the volume of air in the chamber should be considered when calculating the residence time, and thus the volume of the chamber need to be corrected from the snow porosity: $n = 1 - \frac{\rho_{snow}}{\rho_{ice}}$ with ρ_{snow} the snow density in g cm^{-3} calculated by gravimetry, and ρ_{ice} the ice density (0.917 g cm^{-3}).

Snow density ranging from 0.32 to 0.45 g cm^{-3} were measured and consistent with previous observations (Gallet et al., 2011). Snow samples porosity ranging from 0.51 to 0.59, lead to residence times, $\tau = \frac{nV_{FC}}{F_{air}}$, from approximately 3 to 7 min. Previous estimates of NO_x chemical lifetime, τ_{chem}, range between 6.4 h (daily mean) at Halley (Bauguitte et al., 2012) and 8 h (median) at South Pole (Davis et al., 2004).

Based on observed OH and HO_2 during the OPALE campaign, the τ_{chem} for NO_x is estimated to be 3 h at 12:00 local time (LT) and 7 h at 00:00 LT at Dome C (Legrand et al., 2014). NO_x chemical lifetime in the FC experiments is therefore expected to be much longer than the residence time, making the observed NO_x concentrations directly proportional to the NO_x production.

2.3. Instrumentation

The twin instruments used for the NO_x were developed, tested and validated in the laboratory prior the campaign (Barbero et al., 2020). They are based on Incoherent Broad-Band Cavity Enhanced Absorption Spectroscopy (IBBCEAS) for the detection of NO_2 in the 400–475 nm wavelength region. The implementation on the inlet gas line of a compact ozone generator based on water electrolysis allows the measurement

Table 1
Ages of Snow Samples Estimated From a Mean Snow Accumulation in Dome C of Ca. 8.7 cm per Year (Picard et al., 2019)

Type of snow	Estimated age
Drifted snow	–
2–7 cm layer	~3–10 months
10–20 cm layer	~1–2.5 years
30–40 cm layer	~3.5–4.5 years
40–50 cm layer	~4.5–6 years

of NO_x after quantitative conversion of all ambient NO to NO_2 via NO + $O_3 \rightarrow NO_2 + O_2$. The 10-min measurement time used during the experiments permits the acquisition of both the reference and the absorption spectra with detection limits of 54 and 48 x 10^{-12} mol mol^{-1} (3σ) for NO_x and NO_2, respectively, according to an Allan-Werle statistical method (Werle et al., 1993). Additionally, the IBBCEAS instruments were calibrated prior field deployment against a calibrator (FlexStream™ Gas Standards Generator, KINTEK Analytical, Inc.) that produced a stable NO_2 source, covering a large range of concentrations, from the pmol mol^{-1} to nmol mol^{-1} range, with a slope of 1.015 ± 0.006 and a correlation factor of $R^2 = 0.9996$ (Barbero et al., 2020). Field calibrations were made using a NO_2 gas bottle (Air Liquide B10 - NO_2 1 x 10^{-6} mol mol^{-1} in N_2) calibrated prior field deployment against the same calibrator FlexStream™.

The O_3 inside the chamber was monitored using a UV Photometric O_3 analyzer (Thermo Scientific, Model 49i) that achieves 1.5 nmol mol^{-1} (3σ) detection limit within 60 s and was calibrated with an O_3 calibration source (2B Technologies Model 306 Ozone Calibration Source™). This instrument was not solely dedicated to the FC experiments but was connected to a snow tower experiment (Helmig et al., 2020), with one inlet dedicated to the FC experiments: samples were drawn sequentially at flows of typically ~1–2 slpm through a series of switching valves following a 2-h duty cycle of 8 min measurements downstream the FC.

The meteorological data (Figure 1) and information were obtained from the IPEV/PNRA Project, "Routine Meteorological Observation at Station Concordia" (http://www.climantartide.it), using an automatic weather station (AWS-Vaisala Milos 520). The UV radiation was measured with a broadband UV radiometer (Kipp & Zonen-CUV 4, spectral range 305–385 nm) and the intensity of the UV radiation was similar within the experiments. SZA measurements were taken from ground-based SAOZ (Système d'Analyze par Observation Zénitale) as part of the Network for the Detection of Atmospheric Composition Change (NDACC) and the data are publicly available (see http://www.ndacc.org).

Flows were controlled using a piston membrane vacuum pump (Welch™ Standard Duty WOB-LTM Piston Vacuum Pump—Model 2534C-02) and two mass flow controllers (MKS-Mass Flow Controller 10 cm^3 min^{-1} and 10,000 cm^3 min^{-1} at standard conditions: 273.15 K/1,015 hPa), also used for dilution of gas source NO_2 during multi-point calibration of the IBBCEAS on the field (0, 20, 30, 40, 80, 100, 125 and 150 nmol mol^{-1}).

The NO_3^- concentration analysis was repeated twice on each snow samples using an Ion Chromatography (IC) system (Dionex™ ICS—2000, Thermo Scientific) located in the station's laboratory, and snow density was calculated by gravimetry.

2.4. Sampling Strategy

Concordia is a permanent research station on the Antarctic Plateau, and scientific activities occurring in summer regularly involve vehicles, implying possible pollution. For this reason, two types of snow were collected in order to study possible spatial variability: local snow, located in the station's clean area sector (Figure 2) and snow qualified as pristine snow, located 25 km south of the station.

The same protocol was followed on each site: a pit (2 m long, 1 m wide, 1 m deep) was dug using clean shovels. The windward side was then cleaned over the entire depth of the pit. Using a small clean plastic shovel, isotherm boxes (scufa—115 × 35 × 45 cm—cleaned prior sampling) were filled with snow and homogenized by mixing. Each site was sampled three times at different depths: 2–7 cm, 10–20 cm and 40–50 cm for the local snow and 2–7 cm, 10–20 cm and 30–40 cm for the pristine snow. Finally, a sample of drifted snow was collected in the clean area sector on the 2^{nd} of December 2019 during a windy episode, with wind speed of 8.07 ± 0.32 m s^{-1} (1σ) from 10:00 to 15:00 local time. Scufa boxes containing the homogenized samples were then stored in a snow cave in the dark at constant temperature (−55°C). The estimated age of each snow sample, calculated following Picard et al. (2019) is reported in Table 1.

2.5. Typical Experiment

Prior to the experiments, the empty chamber was cleaned by injecting O_3 (~600 nmol mol^{-1}) for 12 h followed by zero-air flushing for another 12 h until reaching stable levels of NO_x (0.068 ± 0.012), nmol mol^{-1}, corresponding to the chamber blank and close to the NO_2 sensitivity of the instrument (Section 2.3).

The snow samples contained in the scufa box was homogenized again and weighed once transferred in the chamber to obtain the density by gravimetry. 8.5–12.0 kg of snow were used to fill up the chamber. The densities calculated for each experiment ranging from 0.32 to 0.45 g cm^{-3} agreed well with previous observations (Gallet et al., 2011).

A mechanical scale (TERAILLON Nautic) installed on a stable surface and leveled was used for the weighing of the snow before and after each experiment. A mean average loss of 1.1% was measured representing about ~100 g of snow sample. The losses observed are not significant in our case for the need of weight corrections.

A total of eight snow samples (≈25 cm^3 each) were taken randomly in the chamber before the FC was sealed, for each experiment. The chamber was then buried in the snowpack, taking care to disturb the surrounding snow as little as possible, and connected to the zero-air flow. The production from the snow was then monitored continuously after the setup of the FC, for 2–4 days.

To investigate the possibility of nitrate stratification and denitrification during the experiments, samples (≈25 cm^3 each) at 2 cm snow depth resolution were collected from the box after each experiment (4 samples for each 2 cm layer were taken resulting in 40 samples).

3. Data Processing

The NO_x measurements from the IBBCEAS were corrected for the chamber blank (0.068 ± 0.012 nmol mol^{-1}) before being further processed for validation. A 2h-running mean was calculated and the standard deviation (σ_{mean}) was determined within the same window. The data falling beyond $2 \times \sigma_{mean}$ were discarded, which resulted in less than 6% rejection. Clouds passing by would impact NO_x and would not be detected as outliers. However, the radiative conditions were the same from 1 day to another during the FC experiments. The measurements were then averaged every 20 min, corresponding to the best performance of the instruments to achieve the ultimate NO_x detection limit of 30 pmol mol^{-1} (Barbero et al., 2020).

As mentioned in Section 2.3, the O_3 inside the chamber was monitored using a UV Photometric O_3 analyzer (Thermo Scientific, Model 49i) connected by tubing to an automatic snow tower platform which housed the switching manifold and the analytical equipment. To eliminate the response time after the switching manifold, only the last three minutes of measurements, when concentrations reach steady-state, were used and averaged, giving one measurement of ozone concentration every 2 h. The data were then interpolated linearly every 20 min to match the resolution of the NO_x measurements.

Snow nitrate concentrations were disregarded when the absolute value of the measurement (NO_3^-) - $[NO_3^-]_{mean}$ was above two standard deviations (2σ). $[NO_3^-]_{mean}$ is the average of repeated measurements for the same sample. 11% of the samples were rejected corresponding to 42 of 392 total samples.

4. Results and Discussions

4.1. Snow Nitrate Content and NO_x Gas Phase Mixing Ratios

During the seven experiments, the O_3 excess with respect to the levels expected from the photochemical NO-NO_2-O_3 equilibrium through the Leighton relationship (Leighton, 1961), was not significant: from 0.7 to 10 nmol mol^{-1} (details of the calculations can be found in Appendix D). Due to this insignificance, we concluded that the potential impact from ozone on our results was negligible, therefore, we decided that there was no need to discuss the ozone data.

Figure 4 shows the nitrate concentration in ng g^{-1} of snow measured in each snow sample before and after the experiments. Drifted snow was found to be up to 30 times more enriched in nitrate than the mean of all the rest of the snow samples, likely due to being blown and stirred by the strong wind (dark blue colors,

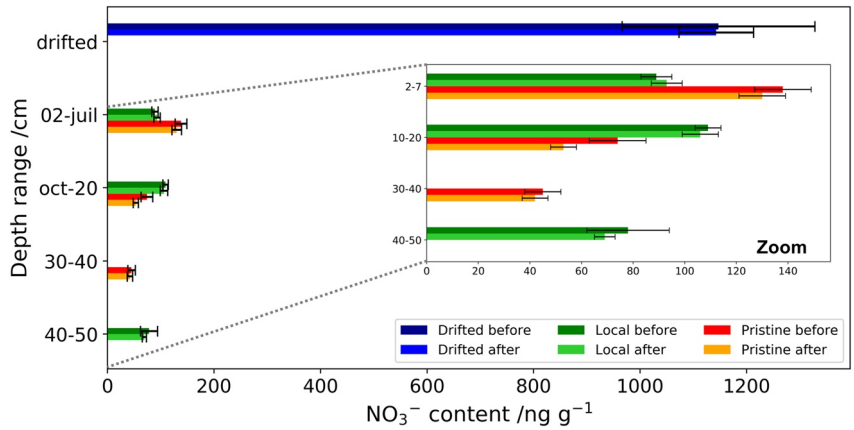

Figure 4. Mixing ratio of NO_3^- contained in the snow [ng g^{-1} of snow] at the two sampling sites before and after the FC experiments. In blue colors, the drifted snow, in red colors, the pristine snow, that is, 25 km South, and in green colors, the local snow. The error bars correspond to one standard deviation, $\pm 1\sigma$, over samples measurements: before experiment = average of 8 samples analyzed twice, and after experiment = average of 40 samples analyzed twice, both after data processing explained in Section 3.

Figure 4). The pristine snow from the 25 km site shows a rapid decrease in nitrate concentrations with depth (red colors, Figure 4), with less than 50 ng g^{-1} of nitrate remaining in the 30–40 cm layer, while local snow shows fairly uniform concentrations over the topmost 50 cm (green colors, Figure 4).

The bottom layers at the two sampling sites do not match in depths due to a sampling error. The exponential decrease of nitrate concentration from the surface to depth is a common feature on the Antarctic plateau, determined by photolysis denitrification occurring in the photic zone. And indeed, the concentrations in the 25 km South snow samples are in agreement with previous observations taken at Dome C shortly after Concordia station construction (Erbland et al., 2013; France et al., 2011).

A part from the top layer sample, the local snow samples appeared enriched in nitrate compare to the pristine snow samples, phenomena probably due to site pollution as demonstrated by Helmig et al. (2020). Additionally, the local sampling area is known to have been very locally contaminated during the previous summer campaign of 2018–2019 by technical activity as shown on Figure F1 given in Appendix F. Therefore, the results given by the local 2–7 cm layer sample, corresponding to a snow aged from the previous summer campaign (Table 1), will be considered with caution.As explained in Section 2.5, four profiles were taken in the flux chamber after each experiment with a 2-cm resolution to observe a potential stratification that would have occurred during the experiments. Samples were analyzed twice with the IC system and the results are shown in Figure 5. The variability observed with depth for the four different profiles of each snow sample is lower than the standard deviation of the measurements. It is reasonable to state that no apparent stratification occurred during the experiments, thus sensible to conclude that our nitrate reservoir is constant.A strong diurnal variability in the NO_x production from the snow is observed for each experiment (Figure 6), with a minimum around midnight and a maximum around local noon, following the daily UV radiation cycle. An apparent proportionality is observed between the nitrate concentrations contained in the snow samples and the amplitude of NO_x mixing ratios produced as a snow with 10 times the concentration of nitrate seems to produce 10 times more NO_x (Figure 6). Second, an exponential decrease in NO_x mixing ratio during the experiments is also observed, potentially due the reservoir denitrification. Assuming one photolyzed molecule of NO_3^- produces one molecule of NO_x (reactions R1 to R5) the denitrification occurring during the experiments represents on average $0.12 \pm 0.08\%$ of the initial amount of nitrate, therefore negligible with respect to the initial nitrate reservoir (more details are provided in Appendix E).

Two main patterns of temporal variations are observed for all experiments in Figure 6: an oscillation driven by the diurnal cycle of UV radiation, called steady-state regime in the following sections, to which is superimposed a slower exponentially decreasing trend with a maximum of NO_x mixing ratio on the first day, called the transitory regime. Below, both regimes are discussed separately. For the stationary regime, a comparison between the different experiments is made with the aim of better characterizing the nitrate

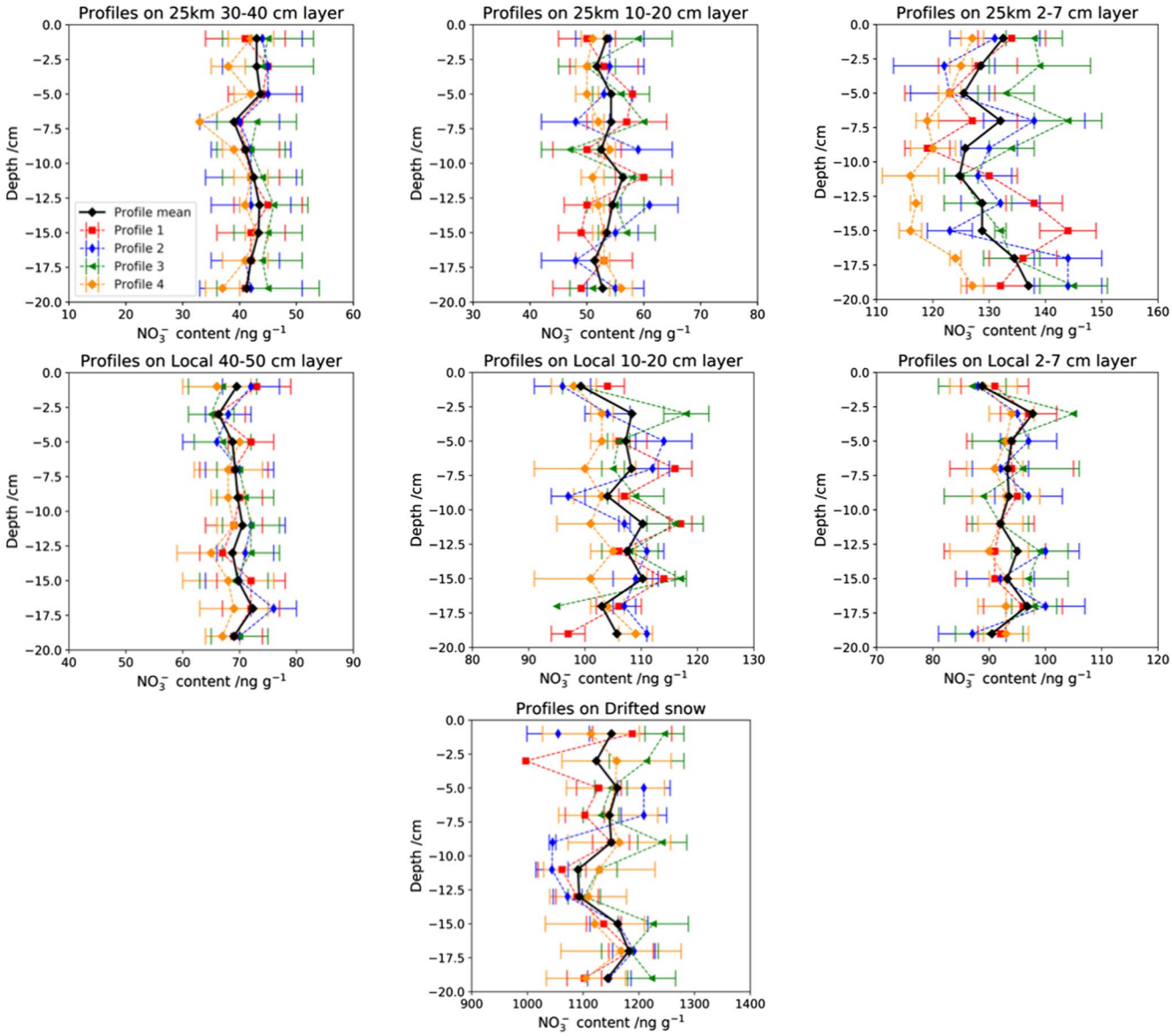

Figure 5. NO_3^- profiles [ng g^{-1}] on the chamber depth for each experiment. Samples were collected with a 2-cm resolution and analyzed twice using the IC system. Blue, red, green and orange colors correspond to four different profiles collected at the end of each experiment, and black colors to the average profile. Error bars correspond to the standard deviation, 1σ, observed for each sample repetition analysis.

photolysis. In a second part, the exponential decrease is studied within the same experiment in an attempt to explain the transitory regime.

4.2. Steady-State Regime Study

Flux chambers are a useful tool for directly measuring production rates of a defined sample. Combining their results with other observations could lead to the estimation of a flux area.

On one hand, the instantaneous NO_x production, P_{NO_x} [molecules s^{-1}], can be calculated based on the measured NO_x mixing ratios, [NO_x] [mol mol^{-1}], and the air-flow passing through the chamber, F_{air} [cm^3 s^{-1}] corrected from the snow porosity n [unit-less], as described in Equation 3:

$$P_{NO_x} = [NO_x] \times F_{air} \times n \times \frac{PN_A}{RT} \quad (3)$$

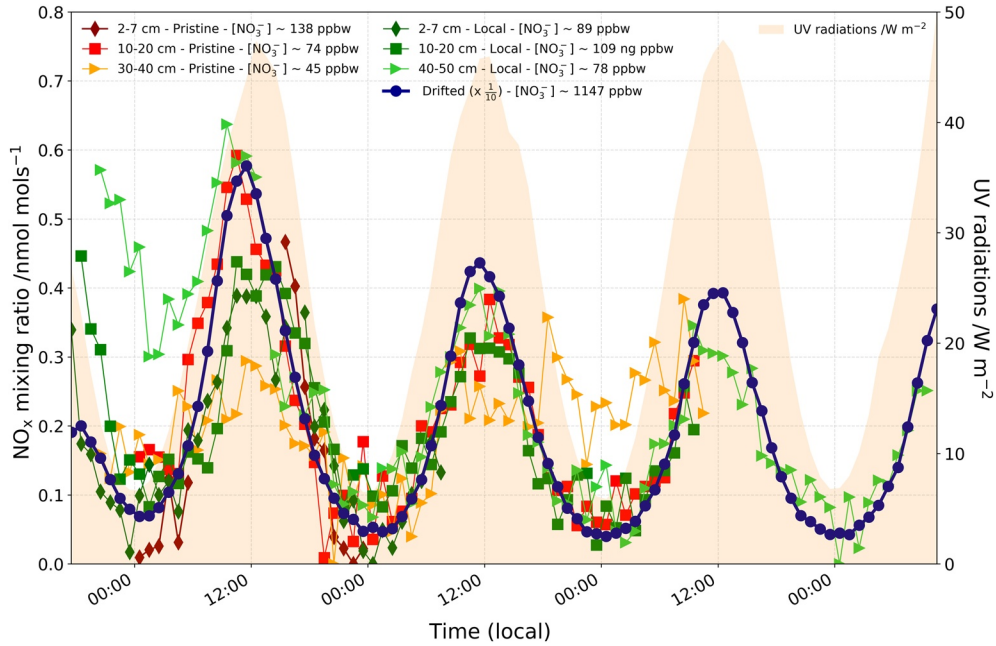

Figure 6. NO_x gas phase mixing ratios measured downstream of the FC [nmol mol^{-1} of air], during FC experiments. Drifted snow mixing ratios (dotted blue curve) are divided by 10. Red colors represent the pristine snows, that is, 25 km South, and green colors the local snows. The intensity of the UV radiation (305–385 nm) was similar within the experiments and the mean value is reported in the shaded orange area. The time is given as local time (UTC + 08:00) where local solar sun maximum is noon.

with N_A Avogadro's Number (6.022×10^{23} molecules mol^{-1}); R, the ideal gas constant (82.06 cm^3 atm mol^{-1} K^{-1}); and P and T taken from the meteorological conditions at Dome C (Section 2.1).

On the other hand, our experiment works as pseudo-first order kinetic where nitrate concentration (NO_3^-) [g g^{-1} of snow], is assumed to be constant and NO_x production, P_{NO_x}, is only driven by the photolysis rate constant $J_{NO_3^-}$ [s^{-1}], following Equation 4:

$$P_{NO_x} = J_{NO_3^-} \times [NO_3^-] \times m_{snow} \times \frac{N_A}{M_{NO_3^-}} \quad (4)$$

with $M_{NO_3^-} = 62.0049$ g mol^{-1} the molar mass of NO_3^-; and m_{snow} [g] the mass of snow sample.

An estimation of the maximum instantaneous P_{NO_x} at local noon for each experiment is made using Equation 3, taking the last day of each experiment as the most representative of the steady-state regime. The results for the maximum NO_x production, $P_{NO_{x-max}}$ [molecules s^{-1}], as well as the results from measurements carried out at Neumayer II Atmospheric Observatory (70°38′S, 8°15′W, 40 m a.s.l) in summer 1997 (Jones et al., 2000), are reported in Table 2.The NO_x production of the FC experiments is proportional to the nitrate concentration initially present in the snow samples as shown in Table 2, where linear regression for the pristine snow shows an $R^2 = 0.691$; and, excluding the local 2–7 cm layer, the linear regression for the local snow shows an $R^2 = 0.999$ (0.659 without the drift sample), note that the linear regressions were calculated with their intercepts forced at zero. This is consistent with previous finding (e.g., Grannas et al., 2007). The local snow sample at 2–7 cm depth exhibits a lower NO_x production, and we strongly suspect that this sample contained absorbing contaminants emitted by the station activities (more details can be found in Appendix F). The NO_x production of snow with similar nitrate concentrations, calculated over one day, is very similar for different snow sources (Figure 7). It can be observed that for two different types of snow of the Antarctic Plateau, the NO_x production is very similar (green triangles and red squares, Figure 7). However, such similarity in production does not exist when it is compared with the Neumayer experiment (Jones et al., 2000), which was located on the western coast of Antarctica but at similar latitude (70°S) as Concordia station (75°S) (solid blue circles, Figure 7). Additionally, the conditions of the Neumayer experiment were

Table 2
Calculated $P_{NO_{x-max}}$ [$\times 10^{11}$ Molecules s^{-1}] From Equation 3 at Solar Noon

Pristine snow samples				Local snow samples				Neumayer[a] snow sample			
Sampling depth	NO_3^- [ng g^{-1}]	$P_{NO_{x-max}}$	Day	Sampling depth	NO_3^- [ng g^{-1}]	$P_{NO_{x-max}}$	Day	Sampling depth	NO_3^- [ng g^{-1}]	$P_{NO_{x-max}}$	Day
30–40 cm	45	1.44	16/12/2019	40–50 cm	78	2.71	13/12/2019	0–20 cm	50	0.31	22-23/02/1999
10–20 cm	74	3.38	06/01/2020	10–20 cm	109	3.34	03/01/2020				
2–7 cm	138	4.05	24-25/12/2019	2–7 cm	89	1.70	22/12/2019				
				drift	1,147	42.82	30/12/2019				

[a]From Jones et al. (2000) experiment on a 20 × 20 × 20 cm block.

different to what was done for this study with the FC experiments. At Neumayer, a snow block of 0.01 m^3 was placed 1 m above the snow surface and exposed to sun light but also to air ventilating all around the block (Jones et al., 2000). As shown in Figure 7, daily mean NO_x production rates from snowpack photolysis are a factor of 10 higher than the values from Jones et al. (2000), which is likely induced by differences in experimental set-up but also in the NO_x snow sources and photolytic mechanisms, that is, differences in radiation fluxes, between East and West Antarctica. The maximum P_{NO_x} observed at Dome C was around 4.0 x 10^{11} molecules s^{-1} while Neumayer's maximum was ~0.3 × 10^{11} molecules s^{-1} for similar UV radiations and snow nitrate concentration. As mentioned previously, the major difficulty in performing the measurement of NO_x fluxes is related to the fact that the latter depends on both transport and photochemical production. Indeed, measurements above snow of NO_x fluxes represent a net flux, thus include contributions from transport and chemical sinks or sources. Our FC design experiments are insensitive to the transport component. Therefore, this ~10 times difference observed at noon could be due, not only to the location of the snow (Coast vs. Plateau, West vs. East) and to the different actinic flux due to different concentrations of snow impurities, but also to this transport component. In addition, Jones et al. (2000) did not observe any change in the nitrate concentration after 50 h of experiment, which supports our conclusion that the nitrate reservoir in the snowpack cannot be photolytically depleted within few hours to few days. Additionally, the snow grain specific surface area (SSA) cannot explain the observed difference in NO_x production (Table 2) between the samples. Indeed, at a depth of 20 cm there was a maximum actinic flux difference of ~40% between the most scattering snow (drifted snow) and the least scattering snow (40–50 cm local snow), Figure 9, which is lower than the observed production differences between the samples.

To estimate the photolysis rate coefficient, $J_{NO_3^-}$ [s^{-1}], Equations 3 and 4 are combined and derived to produce Equation 5.

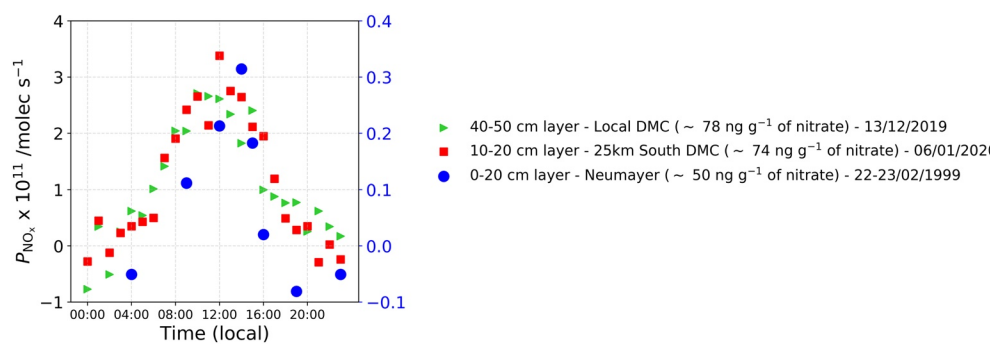

Figure 7. Comparisons of the diurnal variability of snowpack NO_x production rates at different locations for similar nitrate concentrations snows on the Antarctic Plateau: local snow (40–50 cm deep—Concordia station clean area—green triangles (NO_3^-), ~78 ng g^{-1}), pristine snow (10–20 cm deep—25 km south from Concordia station—red squares (NO_3^-), ~74 ng g^{-1}) on the left-hand scale; and measurements over the western coast of Antarctica (blue dots (NO_3^-), ~50 ng g^{-1}), on the right hand-scale.

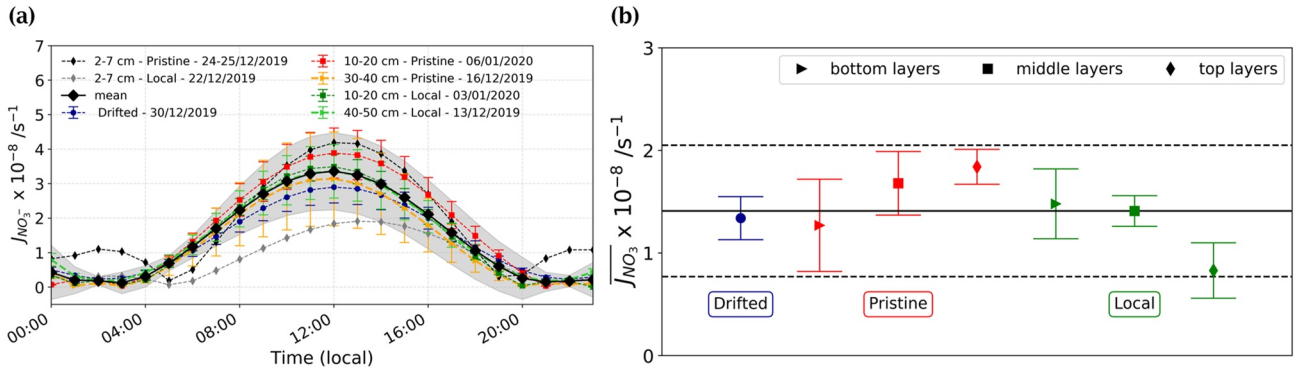

Figure 8. (a) $J_{NO_3^-}$ calculated for each experiment. Dark blue dot represents the drifted snow, red color the pristine snow samples, that is, 25 km South of Concordia station, and green color the local snow samples. Triangles represent the bottom layers (30–40 or 40–50 cm), squares the 10–20 cm layers and diamonds the 2–7 cm layers. The mean $\pm 2\sigma$ is represented by the black diamond and the shaded area and has been calculated from the experiments, excluding the top layers due to: (1) the local top layer is suspected to be locally contaminated; (2) the $J_{NO_3^-}$ of the pristine top layer was reconstructed due to missing data. (b) $\overline{J_{NO_3^-}}$ calculated for each experiment. Dark blue dot represents the drifted snow, red color the pristine snow samples, that is, 25 km South of Concordia station, and green color the local snow samples. Triangles represent the bottom layers (30–40 or 40–50 cm), squares the 10–20 cm layers and diamonds the 2–7 cm layers. The mean $\pm 2\sigma$ calculated from all the experiments, is represented by the solid and dashed black lines.

$$J_{NO_3^-} = \frac{P_{NO_x} \times M_{NO_3^-}}{[NO_3^-] \times m_{snow} \times N_A} \quad (5)$$

with P_{NO_x} [molecules s^{-1}], the NO_x production calculated from Equation 3; $M_{NO_3^-}$ [g mol^{-1}], the molar mass of NO_3^-; (NO_3^-) [g g^{-1} of snow], the amount of nitrate measured in the snow sample; m_{snow} [g], the mass of the snow sample; and N_A [molecules mol^{-1}], Avogadro's number. Results for the steady state regime, that is, last day of each experiment, are presented in Figure 8a. The propagated error from the individual measurement uncertainties are within two times the standard deviation of the calculated values (2σ) for each calculated diurnal $J_{NO_3^-}$. On Figure 8b is shown the daily average photolysis rate coefficients for each experiment, $\overline{J_{NO_3^-}}$ [s^{-1}]. With the exception of the local snow sample at 2–7 cm depth suspected to have been polluted by the station activities, the rest of the measurements lies within the estimated uncertainties, and a mean ($\pm 1\sigma$) $\overline{J_{NO_3^-}}$ of $(1.50 \pm 0.22) \times 10^{-8}$ s^{-1} was found for the 0–20 cm snow layer from the 10/12/2019 to the 07/01/2020, to which further 58% are added to include 3 e-folding depths, leading to a daily ($\pm 1\sigma$) $\overline{J_{NO_3^-}}$ of $(2.37 \pm 0.35) \times 10^{-8}$ s^{-1} over the entire photic zone (0–50 cm) for the same period. Those results suggest the same photolysis rate constant for different types of snow and snow ages as their $\overline{J_{NO_3^-}}$ range from $(1.27 \pm 0.55) \times 10^{-8}$ s^{-1} (16/12/2019) to $(1.84 \pm 0.17) \times 10^{-8}$ s^{-1} (26/12/2019). Additionally, the lifetime of NO_3^- in the chamber against loss by photolysis can be calculated as $\tau_{NO_{3^-photolysis}} = \frac{1}{\overline{J_{NO_3^-}}}$, (Winton et al., 2020; M. Zatko et al., 2016), and is ranging from 2 to 4 years for our FC experiments, much longer than our experiment's duration.

Using the TARTES (Two-streAm Radiative TransfEr in Snow model) optical radiative transfer model (Libois et al., 2013, 2014) coupled with the SBDART (Santa Barbara DISTORT Atmospheric Radiative Transfer) model (Ricchiazzi et al., 1998)) we calculated a theoretical $\sigma_{NO_3^-}(\lambda,T)\phi(T,pH)$ product. Assuming that the black carbon in the snow at Dome C varies between 1 and 5 ng g^{-1} (France et al., 2011) and that it represents all impurities in the model, a $\sigma_{NO_3^-}(\lambda,T)\phi(T,pH)$ product ranging from 1.36×10^{-23} to 1.84×10^{-23} cm^2 $photon^{-1}$ is necessary to estimate a $\overline{J_{NO_{3^-modeled}}}$ ranging from 2.02×10^{-8} s^{-1} to 2.72×10^{-8} s^{-1}, that is, within the 1σ of our observed $\overline{J_{NO_3^-}}$, for $300 < \lambda < 340$ nm.

In gas phase photochemistry, the quantum yield ϕ corresponds to the ratio between the number of dissociations produced and the number of absorbed photons. Nitrate photolysis quantum yield from 0.0015–0.0052

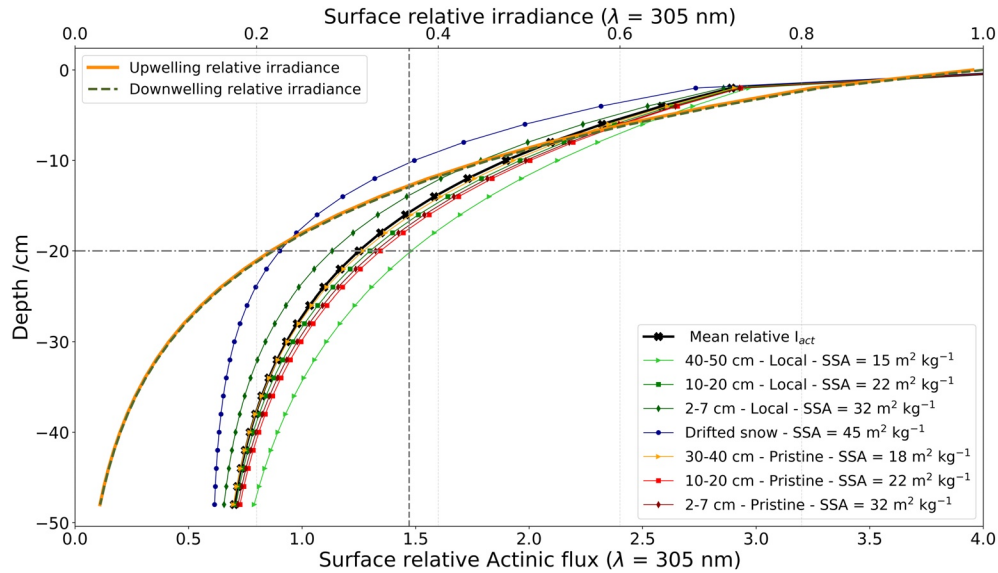

Figure 9. Simulated surface relative actinic fluxes and irradiance for each experiment using TARTES model at 305 nm. The actinic flux describes the number of photons incident at a point, while the irradiance describes the radiant energy crossing a surface. Dotted horizontal line represent the depth of the chamber while the vertical dotted line represents the *e*-folding depth, 20 cm for the 40–50 cm local snow sample and ~12 cm for the drifted snow. Note that surface relative Actinic flux is referenced to the enhanced layer a few mm below the surface, explaining the factor 4.

molecules photon^{-1}, was measured by Chu and Anastasio (2003) on nitrate in ice, and used by M. Zatko et al. (2016) for the NO_x production, but values up to 0.6 molecules photon^{-1} have been measured for HNO_3 adsorbed on ice films in laboratory experiment (Zhu et al., 2010). These disparities are explained by the difficulty, in heterogeneous phase, to define the quantum yield as there is a great diversity of effective absorption cross-sections, which directly influences its calculation. Therefore, it is preferable, in our case (snow-air chemistry), to estimate experimentally the product $\sigma\phi$. In our approach, the use of FC to infer a $\sigma\phi$ product allows to check different snow types, depths and ages and permits to circumvent the uncertainty in both individual terms for NO_3^- on ice, which is needed for models.

Assuming a constant nitrate reservoir as discussed previously, the NO_x production would therefore be a process only driven by the amount of nitrate accessible to the photolysis. Because drifted snow (young) and snow collected in depth (old) possess the same photolysis rate under the same incident light flux despite showing radically different nitrate concentrations, it can reasonably be concluded that nitrate has the same accessibility to photolysis. This implies similar $\sigma_{NO_3^-}(\lambda,T)\phi(T,pH) = (1.60 \pm 0.34) \times 10^{-23}$ cm^2 photon^{-1} (1σ) (with $300 < \lambda < 340$ nm).

Using Chu and Anastasio's (2003) nitrate ion cross-section of 1.20×10^{-20} cm^2 molecules^{-1}, we calculated $\phi(T, pH) \approx 0.0013 \pm 0.0003$ (with $300 < \lambda < 340$ nm) for the measurement period (10/12/2019 to 07/01/2020), which is three times lower than the value usually used in the models. This contradicts previous studies of Davis et al. (2008) and Meusinger et al. (2014) which proposed two nitrate domains: an easy photolabile nitrate fraction (i.e., adsorbed on the surface of ice) and a more difficult to successfully photolyze fraction (i.e., incorporated within the ice crystal lattice). However, our observations are consistent with Bock et al. (2016) and Chan et al. (2018) which proposed a single mechanism responsible for the incorporation of nitrate in the snow at cold sites such as Dome C.

4.3. Transitory Regime Study

The transitory regime represents the decreasing exponential trend observed over the few days of the FC experiments, with a maximum of NO_x gas phase mixing ratios the first day observed in Figure 6. NO_x productions decrease from one day to the next with no special pattern observed between the experiments:

for the drifted snow ($\frac{\Delta P_{NO_x}}{P_{NO_x}}$), represents ~22% for day 1 to day 2 and ~12% for day 2 to day 3 while it represents ~48% and ~21% for the local 40–50 cm layer, respectively, both with an exponential time constant of 22 h.

The total NO_x production ($P_{NO_{x-tot}}$) observed in Figure 6 can be expressed as the sum of the steady state regime production ($P_{NO_{x-steady}}$) and the transitory regime production ($P_{NO_{x-trans}}$), Equation 6. Although the hypothesis of two types of nitrate was disregarded in Section 4.2 because it is not compatible with our findings, where and older snow presents similar photolysis rate coefficient as a younger snow, we still want to question if this transient regime could be produced by a minor family of nitrate that could be depleted more rapidly than the bulk nitrate. Therefore, the hypothesis of two nitrate populations is explored with $P_{NO_{x-steady}}$ already discussed in Section 4.2.

$$P_{NO_{x-tot}} = P_{NO_{x-steady}} + P_{NO_{x-trans}} \tag{6}$$

$P_{NO_{x-trans}}$ is calculated as a function of $J_{NO_{3^-\,trans}}$ and $N_{NO_{3^-_{trans}}}$, following Equation 1 and expressed here by Equation 7:

$$P_{NO_{x-trans}} = J_{NO_{3^-\,trans}} N_{NO_{3^-_{trans}}} \tag{7}$$

We hypothesize that the nitrate photolysis rate at the transitory regime $J_{NO_{3^-\,trans}}$ varies with time and depends on a variety of parameters represented in Equation 2. However, in this experiment, the $\sigma_{NO_3^-}(\lambda)\phi(\lambda, T, pH)$ product is considered constant as the experiments were carried out under the full natural sunlight spectrum and similar temperature diurnal cycle from one day to the next during the experiments. The snow pH is considered to be around 5 and constant over those layers. Furthermore, $I_{act}(\theta, \psi, \lambda, z)$ is considered only θ and ψ dependent as the measurements are integrated over the chamber's depth and under the full spectrum. There is no indication that the actinic flux varies substantially from one day to the next within the chamber's depth; thus, the radiative conditions were the same from one day to another (good weather, homogeneous snow layer, slow metamorphism) and a $J_{NO_{3^-\,trans}}$ that varies from one day to another cannot explain the decrease in NO_x mixing ratios observed for each experiment. Therefore, there are no reasons for a varying $J_{NO_{3^-}}$ from one day to the next within the same experiment and $J_{NO_3^-}$ can be calculated as an integrated parameter over depth and wavelength, Equation 8:

$$J_{NO_3^-}(\lambda) = \sigma_{NO_3^-}\phi\int_{(\theta,\psi)} I_{act}(\theta,\psi)d\theta d\psi \tag{8}$$

It is possible that a thin surface layer is denitrified much faster due to a phenomenon of amplification of the photolysis in this layer, (Traversi et al., 2017), but that was not captured with a coarse sampling resolution of 2 cm.

Simpson et al. (2002) modeled the ratio of the in-snow actinic flux to the incident down-welling actinic flux as a function of extinction optical depth (proportional to depth for homogeneous snow) within the snowpack. Snow increases the actinic flux within the topmost layers of the snowpack, due to the high albedo in the UV region. The actinic flux at the snow surface is equal to the atmospheric actinic flux above the snow, whereas in the first few mm, depending on SZA, the actinic flux is either increased or decreased. For SZA = 0°, the actinic flux is enhanced by the conversion of direct light to diffuse light (Chan et al., 2015). Madronich (1987) argued that the maximum enhancement factor is four times higher than the incident actinic flux. Using the TARTES optical radiative transfer model, relative actinic fluxes for each snow samples at 305 nm were simulated (Figure 9), using specific surface area (SSA) as a function of snow depth following Gallet et al. (2011). No significant differences between the up-welling and the down-welling irradiance are observed (solid orange curve and dotted dashed green curve, Figure 9), making the travel of the light nearly isotropic within the snowpack (i.e., the same properties in every direction), even near the surface.

The actinic flux is thus relatively smooth and ranges between 1.2 and 2.8 times the flux received by the snowpack at 305 nm for the 0–20 cm layer. This variation range is far too small to explain a localized layer with highly photolabile nitrate that would be depleted over the three days of the experiment given the initial abundance of nitrate in all the samples.

Moreover, old snows of 6-year-old should not experience such a transitory regime as the $\tau_{NO_3^-photolysis}$ for those samples were calculated to be ≈ 2–4 years (Section 4.2). This leaves the hypothesis of a strong denitrification.

In Section 4.1, it has been demonstrated that the NO_x production scales with the nitrate concentration in the snow samples. Logically, a decrease in NO_x production will imply a decrease in nitrate concentrations of the same amplitude which was not observed (Section 2.5). Expected NO_3^- losses were calculated for each experiment using Equation 2 from Meusinger et al. (2014), $J^* = -ln\left(\frac{[NO_3^-]_{after}}{[NO_3^-]_{before}}\right)\frac{1}{t_{photolysis}}$, with $t_{photolysis}$ [s] the experiments duration (NO_3^-) [molecules cm^{-3} of snow]; the concentrations before and after the experiments; and J^* [s^{-1}] the apparent photolysis rate constant, calculated in Section 4.2. NO_3^- losses were expecting to be ranging from 0.11 to 4.94 ng g^{-1}, which was not detectable with our IC measurements as it falls below the instrumental precision (Figure 4): the least concentrated snow was measured at 45 ± 7 ng g^{-1} and the most concentrated snow at 1.15 ± 0.18 μg g^{-1}. As the whole thickness of a snow sample undergoes the same exponential I_{act} decrease, and the photolysis rate constant does not depend on the snow age nor location and that no change in nitrate concentration has been observed within the measurement uncertainty, it is difficult to explain this decrease from a variability of $[NO_3^-]_{trans}$ or $J_{NO_3^-trans}$. Thus, we conclude that this transitory regime is potentially due to an experimental interference or artifact.The adsorption of nitric acid (HNO_3) on the walls of the chamber during the installation of the experiment could be an explanation. Zhu et al. (2008) determined the absorption cross-sections of surface-adsorbed HNO_3, noted $HNO_{3-adsorbed}$, in the 290–330 nm region using cavity ring-down spectroscopy. They found that the $HNO_{3-adsorbed}$ absorption cross-section at 305 nm was (1.09 ± 0.17) × 10^{-18} cm^2 $molecules^{-1}$. This makes the absorption cross-section of $HNO_{3-adsorbed}$ ~ 700 times higher than that in the gas phase (HNO_{3-gas}): (1.68 ± 0.19) × 10^{-21} (Zhu et al., 2008), 1.50 × 10^{-21} (Burkholder et al., 1993) and 1.45 × 10^{-21} cm^2 $molecules^{-1}$ at 305 nm (Rattigan et al., 1992). Chu and Anastasio (2003) measured the absorption cross-section of the nitrate ion around 1.2 × 10^{-20} cm^2 $molecules^{-1}$ at Dome C. Therefore, with a cross-section of $HNO_{3-adsorbed}$ about 10^2 times greater than the absorption cross-section of the nitrate ion, the observed exponential decay could indeed be caused by the $HNO_{3-adsorbed}$ on the chamber's walls during the experiments set-up. Additionally, Rajeswari et al. (2016) studied the removal of nitrate ion from aqueous solution and the results obtained in their study illustrate the high adsorption capacity of ion nitrate on polymeric materials. It seems therefore reasonable to estimate similar levels $HNO_{3-adsorbed}$ on PMMA material. A simple calculation giving the number of molecules of $HNO_{3-adsorbed}$ on the chamber's walls needed to produce the amount of NO_x observed in the transitory regime, called $NO_{x-trans}$, support this hypothesis: 1.02 × 10^8 to 3.12 × 10^{10} molecules cm^{-2} of $HNO_{3-adsorbed}$, corresponding to 0.02–7.22 ppt, would be needed to produce this $NO_{x-trans}$ trend by its photolysis destruction. The lifetime of NO_3^- from $HNO_{3-adsorbed}$ in the chamber ranges from 5 to 13 min with a enhanced $J_{NO_3^-trans}$ and assuming that all molecules of $HNO_{3-adsorbed}$ are photolized. Furthermore, Crowley et al. (2010) defined the adsorption equilibrium of HNO_3 on ice, and, for Dome C conditions, an estimation of 14 x 10^{12} molecules cm^{-2} has been established. Therefore, the removal of $HNO_{3-adsorbed}$ would be 1,000 times higher, between approximately 2 to 27 days, making the hypothesis of atmospheric HNO_3 adsorbing on the PMMA walls of the chamber, plausible.

Another hypothesis can also be addressed: the storage of the snow samples before running the FC experiments could as well be involved. As mentioned in Section 2.4, the snow samples were stored in a snow cave, in the dark and at constant temperature (−55 C) for many days. Therefore, it would be possible that mobile species, surface-adsorbed on the walls of the isotherm boxes during sampling had diffused to the surface during storage. Thibert and Dominé (1998) give a parameterization to estimate the diffusion coefficient of HNO_3 in ice as a function of T: $D = 1.37 \times 10^{\frac{-2610}{T}}$ [cm^2 s^{-1}]. $D = 1.5 \times 10^{-12}$ cm^2 s^{-1} in our conditions. The snow samples in their isotherm boxes were stored from 1 to 34 days at most, and the ratio $\frac{\Delta P_{NO_x}}{P_{NO_x}}$ from day 1 to day 2 might seem related to the number of days it stayed in the storage cave, Figure 10a. An estimation of the distance that HNO_3, adsorbed on the walls, could have traveled at −55 C in the snow samples during the storage is calculated using Equation 9.

$$x = \sqrt{q_i D t} \quad (9)$$

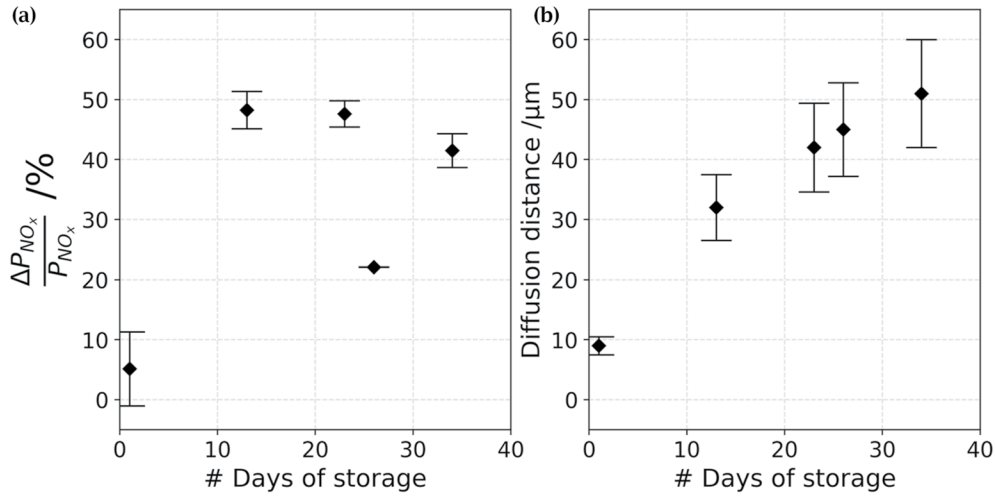

Figure 10. (a) % of NO_x production decrease as a function of the number of days the sample stayed in storage and (b) Estimation of the distance (μm) that HNO_3, adsorbed on the walls, could have traveled in the isotherm box at −55°C.

with x [cm] the mean distance from the starting point that the molecule will have diffused in time t (diffusivity); q_i a numerical constant which depends on dimensionality ($q_i = 2$, 4, or 6, for 1, 2, or 3 dimensional diffusion), here $q_i = 6$ since the molecule is diffusing in every direction; D [$cm^2\ s^{-1}$] the diffusion coefficient previously mentioned and t [s] the storage time. A range of 5–50 μm was found at −55 C (258 K) (Figure 10b).With the available data, both theories proposed to explain the observed transitory regime, that is, HNO_3 surface adsorption during the experiments set-up and/or HNO_3 desorption in the snowpack, could agree with the observations. More experiments with different storage times and longer NO_x gas phase mixing ratios monitoring may be helpful to support our hypothesis. Also, the flushing of the interstitial air contained in the snow samples could be a cause of this transitional regime, and to eliminate this unknown, the answer of monitoring instrument to NO_2 spike tests would help identify possible "dead-air" pockets that may form in the chamber and result in this transitory regime observation.

Note that this does not question the previous conclusions of Section 4.2 as the hypothesis explored tend to confirm an experimental artifact during the set-up of our FC experiments.

4.4. NO_x Flux Estimates and Implications on the Antarctic Plateau

By using open circuit FC with clean air flow injection, instantaneous production can be measured and an estimated average daily production can be obtained. The next step is to estimate the flux per unit of surface area. NO_x flux is estimated at Dome C and an extrapolation to the entire Antarctic continent is proposed in order to obtain a continental N-budget.

4.4.1. Estimated NO_x Flux at Dome C During the Observation Period

NO_x flux is defined as the NO_x production per surface unit area. From Equations 3 and 4, the production was estimated for each experiment and a relatively constant daily $\overline{J_{NO_3^-}}$ of $(2.37 \pm 0.35) \times 10^{-8}\ s^{-1}$ (1σ) was found for a 50 cm snow thickness. In order to estimate the NO_x flux during the observation period at Dome C, Equation 10, a representative NO_3^- concentration in the snowpack is needed. Monthly snow pits at Dome C have been sampled for several years through the programs NITEDC and CAPOXI. A total of 33 measurements from snow pits taken at Dome C during the summer months from 2011 to 2019 were averaged to match the observation period of the FC. This provided a robust estimate of the average nitrate concentration in the first 50 cm of the snowpack for Dome C to 108 ± 8 ng g^{-1} (more information in Appendix G).

$$F_{NO_x} = \int_z^0 \overline{J_{NO_3^-}}[NO_3^-]\frac{\rho_{snow} N_A}{M_{NO_3^-}} dz \quad (10)$$

Table 3
Daily NO_x Flux Estimates From Observations at Dome C

References	F_{NO_x} [x 10^8 molecules cm^{-2} s^{-1}]	$\overline{J_{NO_3^-}}$ [x 10^{-8} s^{-1}]	Observations period	Location
Frey et al. (2013)	6.6	-	23/12/2009–12/01/2010	Dome C
Frey et al. (2013)	8.2 ± 7.4	-	22/12/2009–28/01/2010	Dome C
Frey et al. (2015)	9.4	-	01-08/12/2011	Dome C
Frey et al. (2015)	31	2.93	09-22/12/2011	Dome C
Frey et al. (2015)	13	2.68	23/12/2011–12/01/2012	Dome C
This work (2021)	**4.3 ± 1.2**	**2.37 ± 0.35**	**10/12/2019–07/01/2020**	**Dome C**

with $\overline{J_{NO_3^-}}$ [s^{-1}] the daily photolysis rate constant; $z = -50$ cm; and (NO_3^-) [g g^1] the nitrate concentration of the photic zone. With a snow density of 0.344 ± 0.001 g cm^{-3} for a 0–50 cm layer (Gallet et al., 2011), a daily F_{NO_x} of (4.3 ± 1.2) × 10^8 molecules cm^{-2} s^{-1} was calculated for the entire photic zone at Dome C during the observation period. Previous estimations of snowpack emissions at Dome C are ~1.5 to 7 times higher than what is estimated in this work (Table 3) with a daily photolysis rate constant 12% to 19% lower than the one used by Frey et al. (2015). Frey et al. (2015) scaled $J_{NO_3^-}$ computed with TUV to observations of $J_{NO_3^-}$ from a spectral radiometer. Additionally, Frey et al. (2013, 2015) used observed profiles of $J_{NO_3^-}$ and (NO_3^-) and not an average value over the photic zone. Table 4 hereafter highlights the disparity of the daily average $\overline{F_{NO_x}}$ estimated from field observations and models at both poles.Because of lower likelihood of chemical loss during transport or of potential dilution, $\overline{F_{NO_x}}$ from FC experiment were expected to be larger than the above snow measurements. The *e*-folding depth of the snow samples may be different after the mechanical homogenizing, and a smaller *e*-folding depth would lead to a lower NO_x production therefore lower flux estimation. Using a snow block with intact stratigraphy would allow to reduce the uncertainties on the conversion of P_{NO_x} to F_{NO_x}. Additionally, FC air flow may be only through preferential pathways in the interconnected pore space of the snow matrix, which would result also in a smaller P_{NO_x}. A tracer spike test (e.g., NO_2) would allow to characterize the sample and constrain porosity. However, here we report for the first time the $\overline{F_{NO_x}}$ estimate using our FC approach at Dome C Table 3, and the results from our approach and the flux gradient method (Frey et al., 2013, 2015) fall within the same order of magnitude, confirming the usefulness of the FC approach. A combined experiment of in-snow dynamic FC, as described in this work,

Table 4
Polar NO_x Net Fluxes Measured Above the Snow Surface in Molecules cm^{-2} s^{-1}

	Direct measurement				Model-derived			
	$\overline{F_{NO_x}}$ x 10^8 [molecules cm^{-2} s^{-1}]	Period	Site	Ref	$\overline{F_{NO_x}}$ x 10^8 [molecules cm^{-2} s^{-1}]	Period	Site	Ref
Antarctica	1.3	Feb. 1999	Neumayer	(Jones et al., 2001)	3.2–4.2	Dec. 2003	South Pole	(Wang et al., 2007)
	3.9 ± 0.4	Nov. 2000	South Pole	(Oncley et al., 2004)	3.2–17	Jan.	Dome C	(M. C. Zatko et al., 2013)
	2.42 ± 50%	Jan. 2005	Halley	(Jones et al., 2011)	3.3–22	Jan.	South Pole	(M. C. Zatko et al., 2013)
	1.7	Sum. 2005	Halley	(Bauguitte et al., 2012)	3.5	Sum. 2005	Halley	(Bauguitte et al., 2012)
	8.2 ± 7.4	Jan. 2010	Dome C	(Frey et al., 2015)				
	25 ± 8	Dec. 2011	Dome C	(Frey et al., 2013)				
	42.5	Dec. 2008	WAIS Divide	(Masclin et al., 2013)				
	4.3 ± 1.2	**Dec. 2019**	**Dome C**	**This work (2021)**				
Arctic	2.5	Sum. 2000	Summit	(Honrath et al., 2002)	13–28	Jan.	Summit Pole	(M. C. Zatko et al., 2013)
	≥ 6.7	Apr. 2004	Alert	(Beine et al., 2002)				

with surface-snow dynamic FC, as described in Figure 1 of Ma et al. (2020), would allow to better estimate NO_x production from the snow-pack and the resulted F_{NO_x} released at the surface. Indeed, P_{NO_x} could be used directly in snowpack-air models, which simulate realistic in-snow transport, allowing the community to overcome the difficulty of the quantum yield estimation by directly using the $\sigma\phi$ product from the FC.

4.4.2. Annual NO_x Budget Extrapolated to the Continent

The chemical reactivity of the snowpack and its connection to the overlying oxidative atmosphere is key to understand how it influences the polar environment. A better estimation of the interactions between the snowpack and NO_x emissions offers the perspective of quantifying its importance on a continental scale. Several studies agree that nitrate concentrations in the Antarctic snowpack are generally constant from the coast into the plateau (Becagli et al., 2004; Shi, Buffen, et al., 2018; Shi, Hastings, et al., 2018; Winton et al., 2020). Therefore, the average (NO_3^-) measured at Dome C on the 0–50 cm layer, 108 ± 8 ng g^{-1}, can be taken as a fair approximation for the entire Antarctic continent. To estimate an annual N-budget for the continent, the daily production of NO_x must be calculated for each day of the year. As shown by Equations 2 and 8, J is also a function of SZA, θ affecting the position of the sun over the year, and the sun declination, ψ controlling the length of the day of each day over the year. The term ψ, difficult to be analytically resolved (Finlayson-Pitts & Pitts, 2000), can be approached by calculating it relatively to a reference day, in our case, the 30^{th} of December. here, we used the ratio $L_{day-i} : L_{day-ref}$ with L_{day-i} being the day duration of a day of interest and $L_{day-ref}$ the length of the reference day (more details on the calculation are found in Appendix H). In addition, the variability of the SZA, associated to the maximum amplitude of the NO_x production, should be considered in the extrapolation and it is represented here by a cosine ratio of the solar noon sun's position for the day of interest over the one of reference. This calculation is deduced by Equation 11 hereafter (Finlayson-Pitts & Pitts, 2000; Forsythe et al., 1995).

$$P_{NO_{x-year}} = [NO_3^-]_{mean} V_{cont} \Sigma \overline{J_{NO_{3^-ref}}} \frac{L_{day-i}}{L_{day-ref}} \frac{\cos(\theta_i)}{\cos(\theta_{ref})} \quad (11)$$

θ_i is taken from NDACC and $\overline{J_{NO_{3^-ref}}}$ is (2.37 ± 0.35) x 10^{-8} s^{-1} (1σ). The annual Antarctic continent NO_x budget from the nitrate snow-source calculated from Equation 11 is (0.073 ± 0.017) Tg(nitrate) y^{-1}, or (0.017 ± 0.003) Tg·N y^{-1}. This is a small source on a global scale compared to natural sources, such as biomass burning (7.1 Tg·N y^{-1}), soil (5.6 Tg·N y^{-1}) or lightning (5.0 Tg·N y^{-1}) (Ehhalt et al., 2018). Nevertheless, this comparison on a continental scale with a nitrogen source of the Antarctic atmosphere, such as the stratosphere denitrification, is more useful to understand its significance.

Indeed, the evidence for denitrification in the Antarctic stratosphere is well established since the 90s (Deshler et al., 1991; Fahey et al., 1990; Mulvaney & Wolff, 1993; Salawitch et al., 1989; Santee et al., 1995; Van Allen et al., 1995). Savarino et al. (2007), estimated a N-budget of (0.035 ± 0.015) Tg(nitrate) y^{-1} or (0.008 ± 0.003) Tg·N y^{-1} coming from the stratosphere denitrification, only 2 times less the N-budget of the snowpack denitrification estimated here, making the snowpack source a rather substantial source.

However, McCabe et al. (2007), by studying the oxygen nitrate isotopic composition, suggested that nitrate was the result of a mixture of 25% stratospheric and 75% tropospheric origin, making the total nitrate source around 0.032 Tg·N y^{-1}. Therefore, the recycled nitrogen from the snowpack nitrate photolysis would represent approximately half of the nitrogen atmospheric input. Furthermore, Erbland et al. (2015) simulated that ~20% of the total nitrate mass fluxes, that is, stratospheric and tropospheric inputs as well as photolytic recycling, was exported.

Two scenarios are conceivable: (i) all the NO_x produced by the snowpack denitrification are re-oxidized, making the balance null and closing the nitrate budget in Antarctica; (ii) photolysis destruction of snow nitrate is potentially an important denitrification factor of the Antarctic cryosphere. That said, note that this extrapolation to the continent is a first order estimate as it does not consider the differences on the e-folding depth and the quantum yield variations with temperature and pH, especially at the coast; neither the latitude's differences modifying the ratios used in Equation 11. Indeed, Noro and Takenaka (2020) recently showed that at a coastal site called H128 (69°23'S, 41°34'E) that is located approximately 100 km away from the Japanese Syowa Station in East Antarctica, 50% of the nitrate on surface snow is lost by photolysis. Additionally, they suggest that a photic zone of 45 cm depth is observed at a low impurity coastal

site such as H128, making the photic zone at the coast close to the one observed at the higher plateau. Ideally, a 3-dimensional global chemical transport model of this snowpack source, supported by more FC experiments performed at strategic locations in Antarctica, to constrain the nitrate photolysis and the NO_x production, may be able to answer this question.

5. Conclusion

Flux chambers experiments carried out from December 10^{th} to January 7^{th} during the 2019–2020 campaign at Dome C, Antarctica, allowed to improve our understanding of the mechanisms of snow-contained nitrate photolysis. A common daily average photolysis rate coefficient of $(1.50 \pm 0.22) \times 10^{-8}$ s– 1 (1σ) was estimated for different types of snow samples (different ages and locations) on a 0–20 cm layer. This finding suggests that the photolyzable nitrate present in the snow acts as a uniform source with similar photochemical characteristics and a robust average daily photolysis rate coefficient $\overline{J_{NO_3^-}}$ of $(2.37 \pm 0.35) \times 10^{-8}$ s– 1 (1σ) was estimated for the Antarctic Plateau photic zone (0–50 cm layer).

Daily summer NO_x fluxes at Dome C were estimated to be $(4.3 \pm 1.2) \times 10^8$ molecules cm^{-2} s^{-1} over the observation period, if all NO_x produced were to be carried out of the snowpack, which is 1.5–7 times less than what has been estimated in previous studies at Dome C based on atmospheric gradient measurements, consistent with strong recycling and inter-annual variability of snow pack and atmospheric conditions at a single site.

Observations here are in agreement with Bock et al. (2016) and Chan et al. (2018) theories suggesting that a single dominant incorporation mechanism is controlling the nitrate deposition onto snow (i.e., co-condensation) and that, at cold sites such as Dome C, a young snow will have a similar nitrate distribution in the snow's ice crystal as an older snow.

By extrapolating our FC observations, an annual snow-source NO_x budget of 0.017 ± 0.003 Tg·N y^{-1} was found for Antarctica. Because FC measurements were critical to our findings, we argue that they should be increasingly used across the cryosphere to improve calculations of NO_x budgets as it appears that the recycled nitrogen from the snowpack nitrate photolysis would represent at least half of the net nitrogen input from stratosphere and to the ocean. Knowledge gained in Antarctica may have broader impacts as well, as the re-emission of NO_x (re-noxification) of the atmosphere is a global phenomenon not limited to polar regions (McCalley & Sparks, 2009; Michoud et al., 2015; Su et al., 2011; Seok et al., 2009).

Additional experiments using the methodology and equipment detailed in this work can also better constrain the nitrate photolysis description and the NO_x production estimation, therefore refine parameters for NO_x flux estimation. Their results could help improve uncertainties in the parameterization of the models, in particular the $\sigma\phi$ product, found at Dome C to be $\sigma_{NO_3^-}(\lambda, T)\phi(T, pH) = (1.60 \pm 0.34) \times 10^{-23}$ cm^2 $photon^{-1}$ (1σ) (with $300 < \lambda < 340$ nm), and, using Chu and Anastasio's (2003) nitrate ion cross-section of 1.20×10^{-20} cm^2 $molecules^{-1}$, a $\phi(T, pH) \approx 0.0013 \pm 0.0003$ (with $300 < \lambda < 340$ nm) molecules $photon^{-1}$. Using the $\sigma\phi$ product from the FC is an elegant way to circumvent the uncertainty in both individual terms for NO_3^- on ice. Therefore, with this technique, the NO_x snow-source could be better defined and differences in photolytic mechanics between East and West Antarctica, and between the coast and plateau regions, could be addressed.

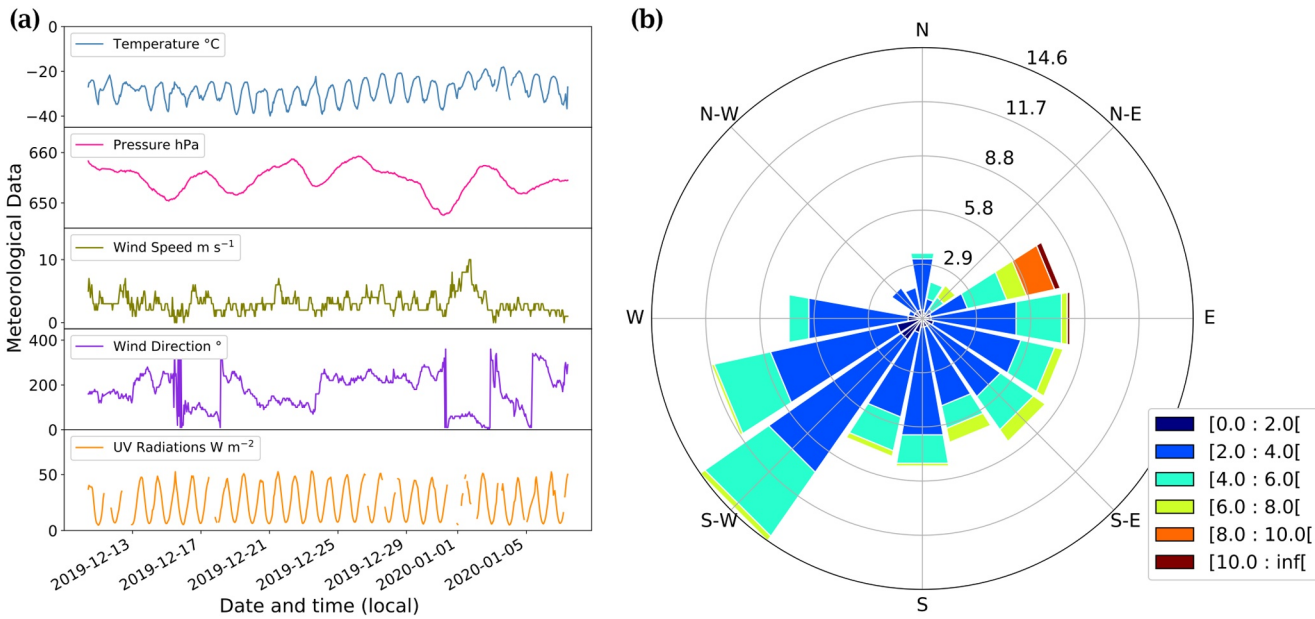

Figure A1. (a) Local meteorological conditions encountered during the experiments measured by the local AWS station (2-m observations) completed with a broadband UV radiometer, spectral range 305–385 nm and (b) the corresponding wind rose in m s^{-1} at Dome C during the FC experiments.

Appendix A: Meteorological Conditions

The meteorological conditions encountered during the 2019–2020 FC experiment ($T_{mean} = -28 \pm 4$ C; $P_{mean} = 654 \pm 3$ hPa; $W_{speed-mean} = 3.4 \pm 1.4$ m s^{-1}; $W_{dir-mean} = 185 \pm 79°$; and $UV_{mean} = 25 \pm 15$ W m^{-2}) were typical of the summer climatology observed at Dome C. Two episodes of strong northeast wind (up to 10 m s^{-1})

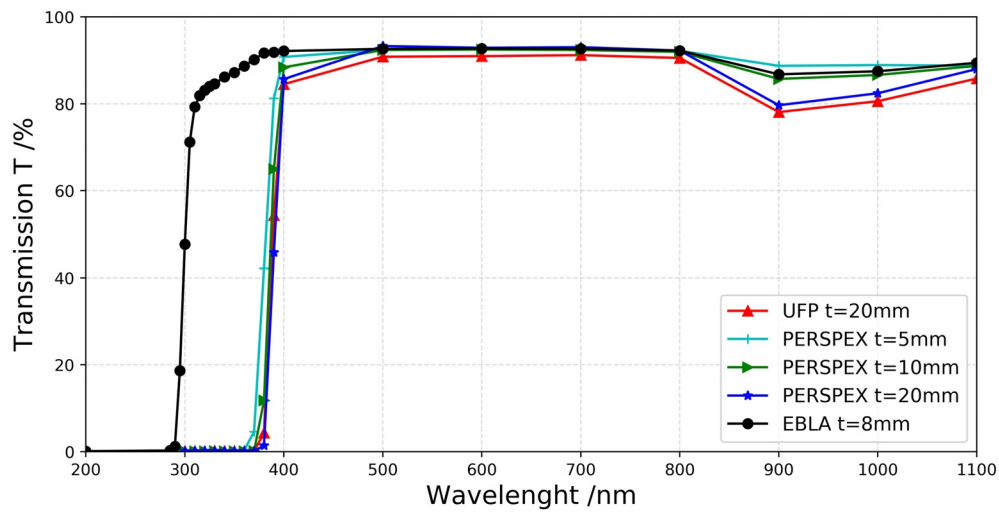

Figure B1. Transparency test of different brands (UFP, PERSPEX and EBLA) and thickness (5, 10, 8, and 20 mm) of PMMA.

occurred mid-December and early January (Figure A1). However, as the FC experiments are not subject to natural air flow, those episodes had no substantial impact on the results.

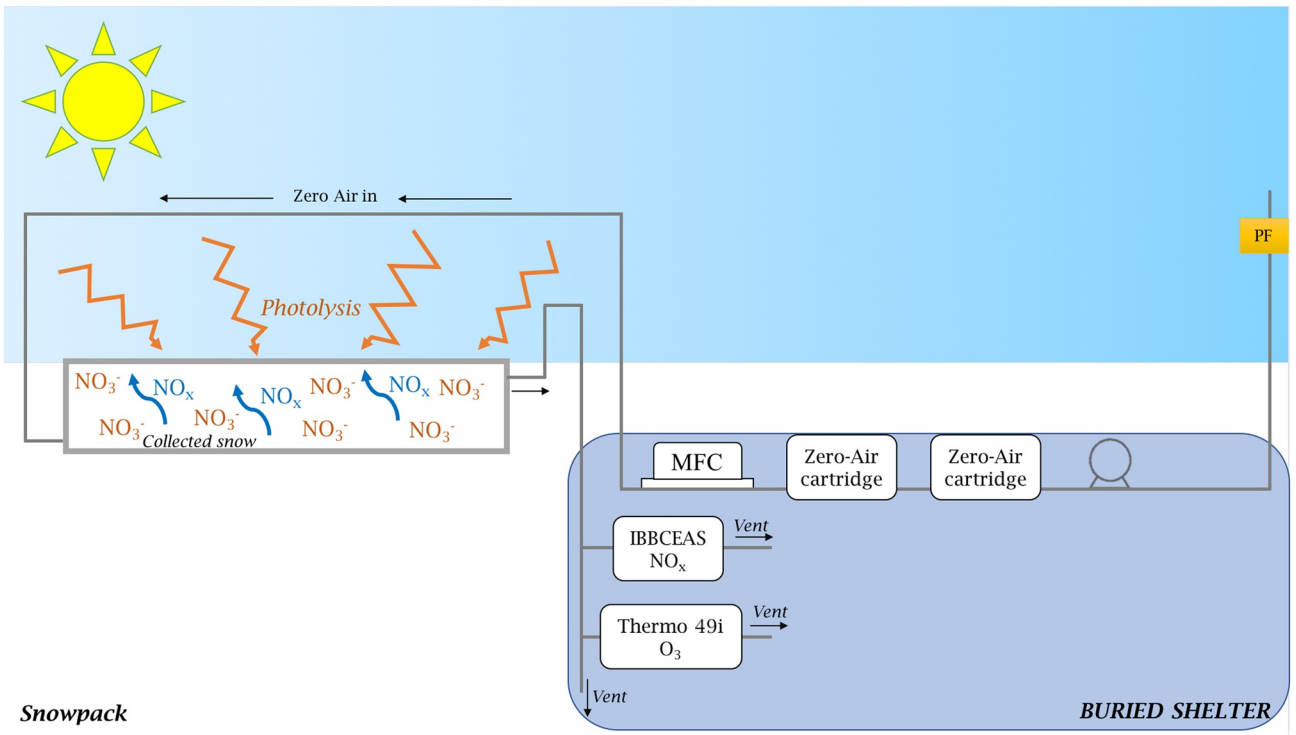

Figure C1. Schematic of the entire experiment and instrumentation: the zero-air flow was produced by pumping external air through two zero-air cartridges mounted in series. A particle filter (PF) was installed at the inlet to prevent any particles entering the pump and the zero-air cartridges. The air flow is controlled using a Mass Flow Controller (MFC) and sent into the chamber. The supply of zero-air drives an equivalent amount of in-chamber air, containing any NO_x produced by photolysis, out through tubing toward the downstream analytical instruments: IBBCEAS and ThermoFisher 49i, for NO_x and O_3 monitoring, respectively.

Appendix B: Transmission Spectra of Polymethyl Methacrylate (PMMA)

The transparency and thickness of different types of PMMA were tested using a 6850 UV/Vis Spectrometer (JenWay Bibby Scientific) ranging from 200 to 1,100 nm. The results (Figure B1) show that the EBLA Brand is the most UV-transparent PMMA available.

Appendix C: Schematic of the Entire Experiment

Figure C1.

Appendix D: Leighton Equilibrium and Ozone Production

Estimations of ozone production in the flux chambers were calculated following Leighton's photo-stationary equilibrium (Leighton, 1961):

$$NO_2 + h\nu\,(\lambda < 420\ \text{nm}) \rightarrow NO + O(^3P) \quad \text{(R.D1)}$$

$$O(^3P) + O_2 + M \rightarrow O_3 + M \quad \text{(R.D2)}$$

$$NO + O_3 \rightarrow NO_2 + O_2 \quad \text{(R.D3)}$$

If equilibrium is reached, then the concentrations of the species involved can be derived following Equation D1:

Table D1
NO_2, NO and O_3 Mixing Ratios and Meteorological Parameters, P and T, at Daily Maximum Observed During the FC Experiments. The Expected O_3 Mixing Ratio From Equation D1 is Reported at the Bottom of the Table

Parameters	Values
NO_2 [nmol mol^{-1}]	0.21–3.46
NO [nmol mol^{-1}]	0.054–0.51
$O_{3_{-measured}}$ [nmol mol^{-1}]	0.7–10
P [atm]	648–655
T [°C]	−29 to −20
$O_{3_{-expected}}$ [nmol mol^{-1}]	2.9–15

$$[O_3] = \frac{J_{NO_2}[NO_2]}{k_{NO+O_3}[NO]} \tag{D1}$$

where J_{NO_2} [s^{-1}] is the photolysis constant rate of reaction (R.D1) and k_{NO+O_3} [cm^3 $molecules^{-1}$ s^{-1}] is the reaction rate of reaction (R.D3). From Atkinson et al. (NIST Kinetics Database), the rate expression of k_{NO+O_3} is given by 1.4 x 10^{-12} $\exp\left(\frac{-10.89[\pm 1.66]}{RT}\right)$ [cm^3 $molecules^{-1}$ s^{-1}] and a J_{NO_2} = 0.016 s^{-1} is taken from (Kukui et al., 2014). (O_3) estimations were calculated at the daily maximum and in the meteorological conditions of the experiments. The O_3 levels expected from the Leighton relationship were ranging from ~3–15 nmol mol^{-1} where 0.7–10 nmol mol^{-1} (Table D1) where measured, confirming that equilibrium was not reached during the FC experiments.

Appendix E: Denitrification

Assuming one photolyzed molecule of NO_3^- produces one molecule of NO_x (Reactions R.1 to R.5 in the manuscript), the denitrification occurring during the experiments can be calculated following Equation E1:

$$\%_{Den} = 100\frac{N_{NO_{x_{total}}}}{N_{NO_3^-{}_{total}}} \tag{E1}$$

with $N_{NO_{x_{total}}}$ the total number of molecules of NO_x emitted during one experiment and $N_{NO_3^-{}_{total}}$, the total number of NO_3^- molecules initially present in the chamber. $N_{NO_3^-{}_{total}}$ and $N_{NO_{x_{total}}}$ are calculated for each experiment following Equations E2 and E3:

$$N_{NO_{x_{total}}} = \rho_{air}\frac{N_A}{M_{NO_x}}[NO_x]V_{FC} \tag{E2}$$

$$N_{NO_3^-{}_{total}} = \rho_{snow}\frac{N_A}{M_{NO_3^-}}[NO_3^-]V_{FC} \tag{E3}$$

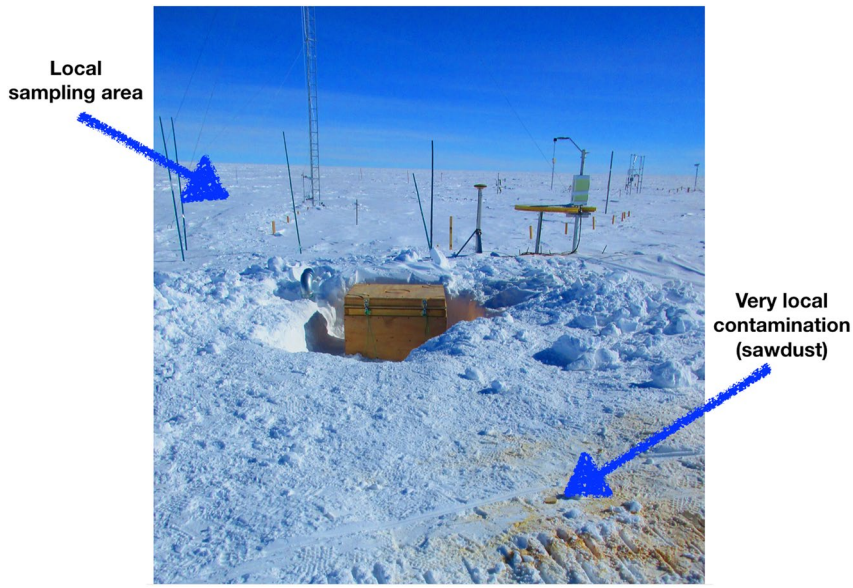

Figure F1. Picture taken in December 2018 showing the very local contamination, leading to the very different behavior of the local 2–7 cm layer sample.

- N_A = Avogadro's number = 6.022×10^{23} molecules mol^{-1}
- M_{NO_x} = Molar mass of NO_x = 76.0155 g mol^{-1}
- $M_{NO_3^-}$ = Molar mass of NO_3^- = 62.0049 g mol^{-1}
- V_{FC} = Chamber volume ~26,500 cm^3
- ρ_{snow} = snow density calculated by gravimetry g cm^{-3}
- ρ_{air} = air density in the snow ~0.929×10^{-3} g cm^{-3} at Dome C

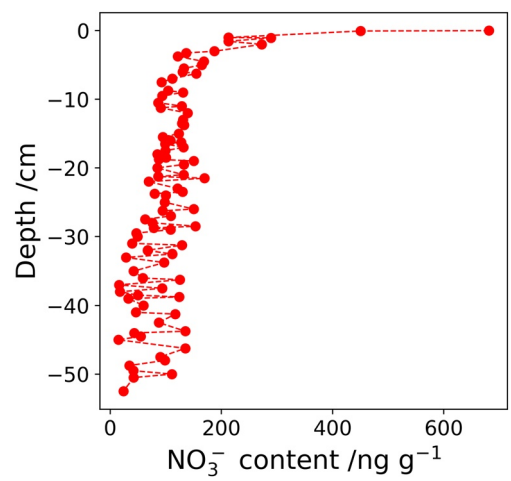

Figure G1. Profile of average NO_3^- concentration [ng g^{-1}] in the near surface snow column at Dome C.

Appendix F: Local 2–7 cm Layer Contamination

During the previous campaign of 2018–2019, a localized contamination occurred near the sampling area during a technical intervention necessary for the safety of the agents to access the snow-covered shelter containing the experiments as shown in Figure F1.

Appendix G: Nitrate Snow Content Profile

Figure G1. As mentioned in the article, snow pits have been sampled at Dome C for several years through the programs NITEDC and CAPOXI. All the data corresponding to the observation period of the FC experiments were averaged giving the profile observed on Figure G1. The average concentration of the photic zone is defined by the area under the averaged curve divided by the depth ($\Delta z = 50$ cm), Equation G1 hereafter, with $z = -50$ cm:

$$[NO_3^-]_{mean} = \frac{\int_z^0 [NO_3^-]dz}{\Delta z} \tag{G1}$$

Using the trapezoidal rule, the average concentration found was $(NO_3^-) = 108 \pm 8$ ng g^{-1}.

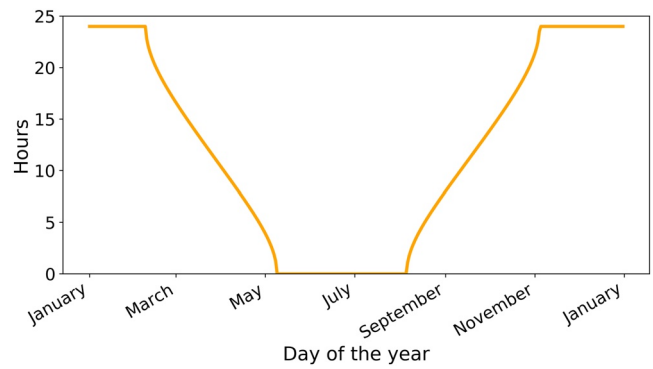

Figure H1. Hours of daylight over the year at Dome C.

Appendix H: Length of Days at Dome C

Figure H1. Daylength calculation was made using a Center for Biosystems Modeling (CBM) model (Forsythe et al., 1995). The model estimates daylength with error less than one minute within 40 degrees of the equator and less than seven minutes within 60°, described by Equations H1, H2 and H3:

$$\theta = 0.2166108 + 2\arctan(0.9671396\tan(0.00860(J - 186))) \tag{H1}$$

$$\phi = \arcsin(0.39795\cos(\theta)) \tag{H2}$$

$$D = 24 - \frac{24}{\pi}\arccos\left[\frac{\sin\left(\frac{p\pi}{180}\right) + \sin\left(\frac{L\pi}{180}\right)\sin(\phi)}{\cos\left(\frac{L\pi}{180}\right)\cos(\theta)}\right] \tag{H3}$$

with θ the predicted revolution angle from the day of the year (J); ϕ the predicted sun's declination angle; D the predicted daylength from Latitude L, here $L = -75.06$. The daylength definition, defined by the position of the sun with respect to the horizon, chosen for this calculation is: sunrise/sunset is when the top of the sun is apparently even with horizon, giving $p = 0.8333$. Figure H1 represents the length of day for one year at Dome C.

Conflict of Interest

The authors declare no conflicts of interest relevant to this study.

Data Availability Statement

The data used in this study are available at https://doi.org/10.5281/zenodo.5285177 with license "Creative Commons Attribution 4.0".

Acknowledgments
The authors greatly thank the reviewers for their thoughtful comments and efforts towards improving the manuscript. The research leading to these results has received funding from: the LabEx OSUG@2020 ("Investissements d'avenir"—ANR10 LABX56); the French National program LEFE (Les Enveloppes Fluides et l'Environnement) via LEFE REACT; the Agence Nationale de la Recherche (ANR) via contract ANR-16-CE01-0011-01 EAIIST; the Foundation BNP-Paribas through its Climate & Biodiversity Initiative program and by the French Polar Institute (IPEV) through programs 1177 (CAPOXI 35–75) and 1169 (EAIIST). Y.H. acknowledges funding support from the National Science Foundation (grant no. 2111428). The meteorological data and information were obtained from IPEV/PNRA Project "Routine Meteorological Observation at Station Concordia" http://www.climantartide.it. The data used in this publication for the irradiations fluxes were obtained from LATMOS, with the help of Florence Goutail et Jean-Pierre Pommereau as part of the Network for the Detection of Atmospheric Composition Change (NDACC) and are publicly available (see http://www.ndacc.org). The authors greatly thank Maria Zatko, Becky Alexander, Shaddy Ahmed, Jennie Thomas and Charles Amory for the inputs on the global atmospheric chemistry and boundary layer modelling. We would like to thank Pete Akers for his help with reviewing the English of the manuscript. Finally, the authors greatly thank the technical staff of the IGE and IPEV for their technical and logistic support in Grenoble and during the field campaign.

References

Barbero, A., Blouzon, C., Savarino, J., Caillon, N., Dommergue, A., & Grilli, R. (2020). A compact incoherent broadband cavity-enhanced absorption spectrometer for trace detection of nitrogen oxides, iodine oxide and glyoxal at levels below parts per billion for field applications. *Atmospheric Measurement Techniques*, *13*(8), 4317–4331. https://doi.org/10.5194/amt-13-4317-2020

Bartels-Rausch, T. & Donaldson, D. J. (2006). HONO and evolution from irradiated nitrate-doped ice and frozen nitrate solutions (preprint). https://doi.org/10.5194/acpd-6-10713-2006

Bauguitte, S. J.-B., Bloss, W. J., Evans, M. J., Salmon, R. A., Anderson, P. S., Jones, A. E., et al. (2012). Summertime NO_x measurements during the CHABLIS campaign: Can source and sink estimates unravel observed diurnal cycles? *Atmospheric Chemistry and Physics*, *12*(2), 989–1002. https://doi.org/10.5194/acp-12-989-2012

Becagli, S., Proposito, M., Benassai, S., Flora, O., Genoni, L., Gragnani, R., et al. (2004). Chemical and isotopic snow variability in East Antarctica along the 2001/02 ITASE traverse. *Annals of Glaciology*, *39*, 473–482. https://doi.org/10.3189/172756404781814636

Beine, H. J., Honrath, R. E., Dominé, F., Simpson, W. R., & Fuentes, J. D. (2002). NO_x during background and ozone depletion periods at Alert: Fluxes above the snow surface. *Journal of Geophysical Research*, *107*(D21), 12. https://doi.org/10.1029/2002JD002082

Berresheim, H., & Eisele, F. L. (1998). Sulfur chemistry in the Antarctic troposphere experiment: An overview of project SCATE. *Journal of Geophysical Research: Atmospheres*, *103*(D1), 1619–1627. https://doi.org/10.1029/97JD00103

Besnard, K., & Pokryszka, Z. (2005). Gases emission monitoring in a post-mining contextIn . *Symposium post mining 2005, Nancy, France* (p. 12). ineris-00972521. https://hal.archives-ouvertes.fr/ineris-00972521/

Blaszczak-Boxe, C. S., & Saiz-Lopez, A. (2018). Nitrate photolysis in ice and snow: A critical review of its multiphase chemistry. *Atmospheric Environment*, *193*, 224–241. https://doi.org/10.1016/j.atmosenv.2018.09.002

Bock, J., Savarino, J., & Picard, G. (2016). Air—snow exchange of nitrate: A modelling approach to investigate physicochemical processes in surface snow at Dome C, Antarctica. *Atmospheric Chemistry and Physics*, *16*(19), 12531–12550. https://doi.org/10.5194/acp-16-12531-2016

Brandt, R. E., & Warren, S. G. (1993). Solar-heating rates and temperature profiles in Antarctic snow and ice. *Journal of Glaciology*, *39*, 12. https://doi.org/10.3189/s0022143000015756

Burkholder, J., Talukdar, A., Ravishankar, A. R., & Susansolomon, A. (1993). Temperature dependence of the HNO_3 UV absorption cross. *Journal of Geophysical Research*, *98*(22), 937–948. https://doi.org/10.1029/93JD02178

Chan, H. G., Frey, M. M., & King, M. D. (2018). Modelling the physical multiphase interactions of HNO_3 between snow and air on the Antarctic Plateau (Dome C) and coast (Halley). *Atmospheric Chemistry and Physics*, *18*(3), 1507–1534. https://doi.org/10.5194/acp-18-1507-2018

Chan, H. G., King, M. D., & Frey, M. M. (2015). The impact of parameterising light penetration into snow on the photochemical production of NO_x and OH radicals in snow. *Atmospheric Chemistry and Physics*, *15*(14), 7913–7927. https://doi.org/10.5194/acp-15-7913-2015

Chu, L., & Anastasio, C. (2003). Quantum yields of hydroxyl radical and nitrogen dioxide from the photolysis of nitrate on ice. *The Journal of Physical Chemistry A*, *107*(45), 9594–9602. https://doi.org/10.1021/jp0349132

Cotel, S., Schäfer, G., Traverse, S., Marzougui-Jaafar, S., Gay, G., & Razakarisoa, O. (2015). Evaluation of VOC fluxes at the soil-air interface using different flux chambers and a quasi-analytical approach. *Water, Air, & Soil Pollution*, *226*(11), 356. https://doi.org/10.1007/s11270-015-2596-y

Cotter, E. S. N., Jones, A. E., & Wolff, E. W. (2003). What controls photochemical NO and NO_2 production from Antarctic snow? Laboratory investigation assessing the wavelength and temperature dependence. *Journal of Geophysical Research*, *108*(D4), 10. https://doi.org/10.1029/2002JD002602

Crowley, J. N., Ammann, M., Cox, R. A., Hynes, R. G., Jenkin, M. E., Mellouki, A., et al. (2010). Evaluated kinetic and photochemical data for atmospheric chemistry: Volume V—heterogeneous reactions on solid substrates. *Atmospheric Chemistry and Physics*, *10*(18), 9059–9223. https://doi.org/10.5194/acp-10-9059-2010

Davis, D., Eisele, F., Chen, G., Crawford, J., Huey, G., Tanner, D., et al. (2004). An overview of ISCAT 2000. *Atmospheric Environment*, *38*(32), 5363–5373. https://doi.org/10.1016/j.atmosenv.2004.05.037

Davis, D., Seelig, J., Huey, G., Crawford, J., Chen, G., Wang, Y., et al. (2008). A reassessment of Antarctic plateau reactive nitrogen based on ANTCI 2003 airborne and ground based measurements. *Atmospheric Environment*, *42*(12), 2831–2848. https://doi.org/10.1016/j.atmosenv.2007.07.039

Deshler, T., Adriani, A., Hofmann, D. J., & Gobbi, G. P. (1991). Evidence for denitrification in the 1990 Antarctic spring stratosphere: II. Lidar and aerosol measurements. *Geophysical Research Letters*, *18*(11), 1999–2002. https://doi.org/10.1029/91GL02311

Domine, F., Albert, M., Huthwelker, T., & Simpson, W. R. (2008). Snow physics as relevant to snow photochemistry. *Atmospheric Chemistry and Physics*, *8*, 171–208. https://doi.org/10.5194/acp-8-171-2008

Domine, F., & Shepson, P. B. (2002). Air-snow interactions and atmospheric chemistry. *Science*, *297*(5586), 1506–1510. https://doi.org/10.1126/science.1074610

Ehhalt, D., Prather, M., Dentener, F., Derwent, R., Dlugokencky, E., Holland, E., et al. (2018). *Atmospheric chemistry and greenhouse gases* (pp. 240–287). IPCC. https://www.ipcc.ch/report/ar3/wg1/chapter-4-atmospheric-chemistry-and-greenhouse-gases/

Eklund, B. (1992). Practical guidance for flux chamber measurements of fugitive volatile organic emission rates. *Journal of the Air & Waste Management Association*, *42*(12), 1583–1591. https://doi.org/10.1080/10473289.1992.10467102

Erbland, J., Savarino, J., Morin, S., France, J. L., Frey, M. M., & King, M. D. (2015). Air-snow transfer of nitrate on the East Antarctic Plateau—Part 2: An isotopic model for the interpretation of deep ice-core records. *Atmospheric Chemistry and Physics*, *15*(20), 12079–12113. https://doi.org/10.5194/acp-15-12079-2015

Erbland, J., Vicars, W. C., Savarino, J., Morin, S., Frey, M. M., Frosini, D., et al. (2013). Air—snow transfer of nitrate on the East Antarctic Plateau—Part 1: Isotopic evidence for a photolytically driven dynamic equilibrium in summer. *Atmospheric Chemistry and Physics*, *13*(13), 6403–6419. https://doi.org/10.5194/acp-13-6403-2013

Fahey, D. W., Kelly, K. K., Kawa, S. R., Tuck, A. F., Loewenstein, M., Chan, K. R., & Heidt, L. E. (1990). Observations of denitrification and dehydration in the winter polar stratospheres. *Nature*, *344*, 321–324. https://doi.org/10.1038/344321a0

Finlayson-Pitts, B. J., & Pitts, J. N. (2000). Chapter 7—Chemistry of inorganic nitrogen compounds. In *Chemistry of the upper and lower atmosphere* (pp. 264–293). Academic Press. https://doi.org/10.1016/B978-0-12-257060-5.X5000-X

Forsythe, W. C., Rykiel, E. J., Stahl, R. S., Wu, H.-i., & Schoolfield, R. M. (1995). A model comparison for daylength as a function of latitude and day of year. *Ecological Modelling*, *80*(1), 87–95. https://doi.org/10.1016/0304-3800(94)00034-F

France, J. L., King, M. D., Frey, M. M., Erbland, J., Picard, G., Preunkert, S., et al. (2011). Snow optical properties at Dome C (Concordia), Antarctica; implications for snow emissions and snow chemistry of reactive nitrogen. *Atmospheric Chemistry and Physics*, *11*(18), 9787–9801. https://doi.org/10.5194/acp-11-9787-2011

Frey, M. M., Brough, N., France, J. L., Anderson, P. S., Traulle, O., King, M. D., et al. (2013). The diurnal variability of atmospheric nitrogen oxides (NO and NO_2) above the Antarctic Plateau driven by atmospheric stability and snow emissions. *Atmospheric Chemistry and Physics*, *13*(6), 3045–3062. https://doi.org/10.5194/acp-13-3045-2013

Frey, M. M., Roscoe, H. K., Kukui, A., Savarino, J., France, J. L., King, M. D., et al. (2015). Atmospheric nitrogen oxides (NO and NO_2) at Dome C, East Antarctica, during the OPALE campaign. *Atmospheric Chemistry and Physics*, *15*(14), 7859–7875. https://doi.org/10.5194/acp-15-7859-2015

Gallet, J.-C., Domine, F., Arnaud, L., Picard, G., & Savarino, J. (2011). Vertical profile of the specific surface area and density of the snow at Dome C and on a transect to Dumont D'Urville, Antarctica—albedo calculations and comparison to remote sensing products. *The Cryosphere*, *5*(3), 631–649. https://doi.org/10.5194/tc-5-631-2011

Grannas, A. M., Jones, A. E., Dibb, J., Ammann, M., Anastasio, C., Beine, H. J., et al. (2007). An overview of snow photochemistry: Evidence, mechanisms and impacts. *Atmospheric Chemistry and Physics*, *7*, 4329–4373. https://doi.org/10.5194/acp-7-4329-2007

Grilli, R., Legrand, M., Kukui, A., Méjean, G., Preunkert, S., & Romanini, D. (2013). First investigations of IO, BrO, and NO_2 summer atmospheric levels at a coastal East Antarctic site using mode-locked cavity enhanced absorption spectroscopy. *Geophysical Research Letters*, *40*(4), 791–796. https://doi.org/10.1002/grl.50154

Helmig, D., Liptzin, D., Hueber, J., & Savarino, J. (2020). Impact of exhaust emissions on chemical snowpack composition at Concordia Station, Antarctica. *The Cryosphere*, *14*(1), 199–209. https://doi.org/10.5194/tc-14-199-2020

Honrath, R. E., Guo, S., Peterson, M. C., Dziobak, M. P., Dibb, J. E., & Arsenault, M. A. (2000). Photochemical production of gas phase NO_x from ice crystal NO_3^-. *Journal of Geophysical Research: Atmospheres*, *105*(D19), 24183–24190. https://doi.org/10.1029/2000JD900361

Honrath, R. E., Lu, Y., Peterson, M. C., Dibb, J. E., Arsenault, M. A., Cullen, N. J., & Steffen, K. (2002). Vertical fluxes of NO_x, HONO, and HNO_3 above the snowpack at Summit, Greenland. *Atmospheric Environment*, *36*, 2629–2640. https://doi.org/10.1016/S1352-2310(02)00132-2

Honrath, R. E., Peterson, M. C., Guo, S., Dibb, J. E., Shepson, P. B., & Campbell, B. (1999). Evidence of NO_x production within or upon ice particles in the Greenland snowpack. *Geophysical Research Letters*, *26*(6), 695–698. https://doi.org/10.1029/1999GL900077

Jones, A. E., Weller, R., Anderson, P. S., Jacobi, H.-W., Wolff, E. W., Schrems, O., & Miller, H. (2001). Measurements of NO_x emissions from the Antarctic snowpack. *Geophysical Research Letters*, *28*(8), 1499–1502. https://doi.org/10.1029/2000GL011956

Jones, A. E., Weller, R., Wolff, E. W., & Jacobi, H. W. (2000). Speciation and rate of photochemical NO and NO_2 production in Antarctic snow. *Geophysical Research Letters*, *27*(3), 345–348. https://doi.org/10.1029/1999GL010885

Jones, A. E., Wolff, E. W., Ames, D., Bauguitte, S. J.-B., Clemitshaw, K. C., Fleming, Z., et al. (2011). The multi-seasonal NO_y budget in coastal Antarctica and its link with surface snow and ice core nitrate: Results from the CHABLIS campaign. *Atmospheric Chemistry and Physics*, *11*(17), 9271–9285. https://doi.org/10.5194/acp-11-9271-2011

Kukui, A., Legrand, M., Preunkert, S., Frey, M. M., Loisil, R., Gil Roca, J., et al. (2014). Measurements of OH and RO_2 radicals at Dome C, East Antarctica. *Atmospheric Chemistry and Physics*, *14*(22), 12373–12392. https://doi.org/10.5194/acp-14-12373-2014

Legrand, M., Preunkert, S., Frey, M., Bartels-Rausch, T., Kukui, A., King, M. D., et al. (2014). Large mixing ratios of atmospheric nitrous acid (HONO) at Concordia (East Antarctic Plateau) in summer: A strong source from surface snow? *Atmospheric Chemistry and Physics*, *14*(18), 9963–9976. https://doi.org/10.5194/acp-14-9963-2014

Leighton, P. A. (1961). *Photochemistry of air pollution*.New York: Academic Press. https://www.elsevier.com/books/photochemistry-of-air-pollution/leighton/978-0-12-442250-6

Lenschow, D. (1995). In P. A. Matson, & R. C. Hariss (Eds.), *Micrometeorological techniques for measuring biosphere-atmosphere trace gas exchange* (Vol. 126–163). Oxford: Blackwell Science. http://n2t.net/ark:/85065/d7gm88qf

Libois, Q., Picard, G., Dumont, M., Arnaud, L., Sergent, C., Pougatch, E., & Vial, D. (2014). Experimental determination of the absorption enhancement parameter of snow. *Journal of Glaciology*, *60*(222), 714–724. https://doi.org/10.3189/2014JoG14J015

Libois, Q., Picard, G., France, J. L., Arnaud, L., Dumont, M., Carmagnola, C. M., et al. (2013). Influence of grain shape on light penetration in snow. *The Cryosphere*, *7*, 1803–1818. https://doi.org/10.5194/tc-7-1803-2013

Ma, J., McHugh, T., & Eklund, B. (2020). Flux chamber measurements should play a more important role in contaminated site management . *Environmental Science & Technology*, *54*(19), 11645–11647. https://doi.org/10.1021/acs.est.0c04078

Madronich, S. (1987). Photodissociation in the atmosphere 1. Actinic flux and the effects of ground reflections and clouds. *Journal of Geophysical Research*, *92*(D8), 9740–975214. https://doi.org/10.1029/JD092iD08p09740

Masclin, S., Frey, M. M., Rogge, W. F., & Bales, R. C. (2013). Atmospheric nitric oxide and ozone at the WAIS Divide deep coring site: A discussion of local sources and transport in West Antarctica. *Atmospheric Chemistry and Physics*, *13*(17), 8857–8877. https://doi.org/10.5194/acp-13-8857-2013

Mauldin, R., Kosciuch, E., Eisele, F., Huey, G., Tanner, D., Sjostedt, S., et al. (2010). South Pole Antarctica observations and modeling results: New insights on HO_x radical and sulfur chemistry. *Atmospheric Environment*, *44*(4), 572–581. https://doi.org/10.1016/j.atmosenv.2009.07.058

Mauldin, R. L., Eisele, F. L., Tanner, D. J., Kosciuch, E., Shetter, R., Lefer, B., et al. (2001). Measurements of OH, H_2SO_4 and MSA at the South Pole during ISCAT. *Geophysical Research Letters*, *28*(19), 3629–3632. https://doi.org/10.1029/2000GL012711

Mauldin, R. L., Kosciuch, E., Henry, B., Eisele, F. L., Shetter, R., Lefer, B., et al. (2004). Measurements of OH, HO_2 + RO_2, H_2SO_4, and MSA at the South Pole during ISCAT 2000. *Atmospheric Environment*, *38*(32), 5423–5437. https://doi.org/10.1016/j.atmosenv.2004.06.031

McCabe, J. R., Thiemens, M. H., & Savarino, J. (2007). A record of ozone variability in South Pole Antarctic snow: Role of nitrate oxygen isotopes. *Journal of Geophysical Research*, *112*(D12), D12303. https://doi.org/10.1029/2006JD007822

McCalley, C. K., & Sparks, J. P. (2009). Abiotic gas formation drives nitrogen loss from a desert ecosystem. *Science*, *326*(5954), 837–840. https://doi.org/10.1126/science.1178984

Meusinger, C., Berhanu, T. A., Erbland, J., Savarino, J., & Johnson, M. S. (2014). Laboratory study of nitrate photolysis in Antarctic snow. I. Observed quantum yield, domain of photolysis, and secondary chemistry. *The Journal of Chemical Physics*, *140*(24), 244305. https://doi.org/10.1063/1.4882898

Michoud, V., Doussin, J.-F., Colomb, A., Afif, C., Borbon, A., Camredon, M., et al. (2015). Strong HONO formation in a suburban site during snowy days. *Atmospheric Environment*, *116*, 155–158. https://doi.org/10.1016/j.atmosenv.2015.06.040

Mulvaney, R., & Wolff, E. W. (1993). Evidence for winter/spring denitrification of the stratosphere in the nitrate record of Antarctic firn cores. *Journal of Geophysical Research: Atmospheres*, *98*(D3), 5213–5220. https://doi.org/10.1029/92JD02966

Noro, K., & Takenaka, N. (2020). Post-depositional loss of nitrate and chloride in Antarctic snow by photolysis and sublimation: A field investigation. *Polar Research*, *39*. https://doi.org/10.33265/polar.v39.5146

Oncley, S., Buhr, M., Lenschow, D., Davis, D., & Semmer, S. (2004). Observations of summertime NO fluxes and boundary-layer height at the South Pole during ISCAT 2000 using scalar similarity. *Atmospheric Environment*, *38*(32), 5389–5398. https://doi.org/10.1016/j.atmosenv.2004.05.053

Palchetti, L., Bianchini, G., Di Natale, G., & Del Guasta, M. (2015). Far-Infrared radiative properties of water vapor and clouds in antarctica. *Bulletin of the American Meteorological Society*, *96*(9), 1505–1518. https://doi.org/10.1175/BAMS-D-13-00286.1

Picard, G., Arnaud, L., Caneill, R., Lefebvre, E., & Lamare, M. (2019). Observation of the process of snow accumulation on the Antarctic Plateau by time lapse laser scanning. *The Cryosphere*, *13*(7), 1983–1999. https://doi.org/10.5194/tc-13-1983-2019

Pokryszka, Z., & Tauzièdе, C. (1999). Method of measuring surface emissions of methane. *International Conference on Latest Achievements in the Field of Mine Ventilation Fire and Methane Hazrad Fighting* (pp. 277–283).

Preunkert, S., Ancellet, G., Legrand, M., Kukui, A., Kerbrat, M., Sarda-Estève, R., et al. (2012). Oxidant Production over Antarctic Land and its Export (OPALE) project: An overview of the 2010–2011 summer campaign. *Journal of Geophysical Research: Atmospheres*, *117*(D15), 307–319. https://doi.org/10.1029/2011JD017145

Rajeswari, A., Amalraj, A., & Pius, A. (2016). Adsorption studies for the removal of nitrate using chitosan/PEG and chitosan/PVA polymer composites. *Journal of Water Process Engineering*, *9*, 123–134. https://doi.org/10.1016/j.jwpe.2015.12.002

Rattigan, O., Lutman, E., Jones, R. L., & Coxt, R. A. (1992). Temperature-dependent absorption cross-sections of gaseous nitric acid and methyl nitrate. *Journal of Photochemistry and Photobiology A: Chemistry*, *66*, 313–326. https://doi.org/10.1002/bbpc.19920960331

Ricchiazzi, P., Yang, S., Gautier, C., & Sowle, D. (1998). SBDART: A research and teaching software tool for plane-parallel radiative transfer in the Earth'S atmosphere. *Bulletin of the American Meteorological Society*, *79*(10), 14. https://doi.org/10.1175/1520-0477(1998)079<2101:SARATS>2.0.CO;2

Salawitch, R. J., Gobbi, G. P., Wofsy, S. C., & McElroy, M. B. (1989). Denitrification in the Antarctic stratosphere. *Nature*, *339*, 525–527. https://doi.org/10.1038/339525a0

Santee, M. L., Read, W. G., Waters, J. W., Froidevaux, L., Manney, G. L., Flower, D. A., et al. (1995). Interhemispheric differences in polar stratospheric HNO_3, H_2O, ClO, and O_3. *Science*, *267*, 849–852. https://doi.org/10.1126/science.267.5199.849

Savarino, J., Kaiser, J., Morin, S., Sigman, D. M., & Thiemens, M. H. (2007). Nitrogen and oxygen isotopic constraints on the origin of atmospheric nitrate in coastal Antarctica. *Atmospheric Chemistry and Physics*, *7*, 1925–1945. https://doi.org/10.5194/acp-7-1925-2007

Savarino, J., Vicars, W. C., Legrand, M., Preunkert, S., Jourdain, B., Frey, M. M., et al. (2016). Oxygen isotope mass balance of atmospheric nitrate at Dome C, East Antarctica, during the OPALE campaign. *Atmospheric Chemistry and Physics*, *16*(4), 2659–2673. https://doi.org/10.5194/acp-16-2659-2016

Savitskiy, G. B., & Lessing, V. M. (1979). Tropospheric jet streams in the Antarctic. *Polar Geography*, *3*(3), 157–160. https://doi.org/10.1080/10889377909377113

Scheutz, C., Bogner, J., Chanton, J. P., Blake, D., Morcet, M., Aran, C., & Kjeldsen, P. (2008). Atmospheric emissions and attenuation of non-methane organic compounds in cover soils at a French landfill. *Waste Management*, *28*(10), 1892–1908. https://doi.org/10.1016/j.wasman.2007.09.010

Seok, B., Helmig, D., Williams, M. W., Liptzin, D., Chowanski, K., & Hueber, J. (2009). An automated system for continuous measurements of trace gas fluxes through snow: An evaluation of the gas diffusion method at a subalpine forest site, Niwot Ridge, Colorado. *Biogeochemistry*, *95*(1), 95–113. https://doi.org/10.1007/s10533-009-9302-3

Shi, G., Buffen, A., Ma, H., Hu, Z., Sun, B., Li, C., et al. (2018). Distinguishing summertime atmospheric production of nitrate across the East Antarctic Ice Sheet. *Geochimica et Cosmochimica Acta*, *231*, 1–14. https://doi.org/10.1016/j.gca.2018.03.025

Shi, G., Hastings, M. G., Yu, J., Ma, T., Hu, Z., An, C., et al. (2018). Nitrate deposition and preservation in the snowpack along a traverse from coast to the ice sheet summit (Dome A) in East Antarctica. *The Cryosphere*, *12*(4), 1177–1194. https://doi.org/10.5194/tc-12-1177-2018

Sihota, N. J., Singurindy, O., & Mayer, K. U. (2010). CO_2-Efflux Measurements for evaluating source zone natural attenuation rates in a petroleum hydrocarbon contaminated aquifer. *Environmental Science & Technology*, *45*, 482–488. https://doi.org/10.1021/es1032585

Simpson, W. R., King, M. D., Beine, H. J., Honrath, R. E., & Zhou, X. (2002). Radiation-transfer modeling of snow-pack photochemical processes during ALERT 2000. *Atmospheric Environment*, *36*(15–16), 2663–2670. https://doi.org/10.1016/S1352-2310(02)00124-3

Su, H., Cheng, Y., Oswald, R., Behrendt, T., Trebs, I., Meixner, F. X., et al. (2011). Soil nitrite as a source of atmospheric HONO and OH radicals. *Science*, *333*, 1616–1618. https://doi.org/10.1126/science.1207687

Thibert, E., & Dominé, F. (1998). Thermodynamics and kinetics of the solid solution of HNO_3 in ice. *The Journal of Physical Chemistry B*, *102*(22), 4432–4439. https://doi.org/10.1021/jp980569a

Thomas, J. L., Dibb, J. E., Huey, L. G., Liao, J., Tanner, D., Lefer, B., et al. (2012). Modeling chemistry in and above snow at Summit, Greenland—Part 2: Impact of snowpack chemistry on the oxidation capacity of the boundary layer. *Atmospheric Chemistry and Physics*, *12*(14), 6537–6554. https://doi.org/10.5194/acp-12-6537-2012

Thomas, J. L., Stutz, J., Lefer, B., Huey, L. G., Toyota, K., Dibb, J. E., & von Glasow, R. (2011). Modeling chemistry in and above snow at Summit, Greenland—Part 1: Model description and results. *Atmospheric Chemistry and Physics*, *11*(10), 4899–4914. https://doi.org/10.5194/acp-11-4899-2011

Tillman, F. D., Choi, J.-W., & Smith, J. A. (2003). A comparison of direct measurement and model simulation of total flux of volatile organic compounds from the subsurface to the atmosphere under natural field conditions: Measurement and simulation of VOC flux. *Water Resources Research*, *39*(10). https://doi.org/10.1029/2003WR002098

Traversi, R., Becagli, S., Brogioni, M., Caiazzo, L., Ciardini, V., Giardi, F., et al. (2017). Multi-year record of atmospheric and snow surface nitrate in the central Antarctic plateau. *Chemosphere*, *172*, 341–354. https://doi.org/10.1016/j.chemosphere.2016.12.143

Van Allen, R., Liu, X., & Murcray, F. J. (1995). Seasonal variation of atmospheric nitric acid over the South Pole in 1992. *Geophysical Research Letters*, *22*(1), 49–52. https://doi.org/10.1029/94GL02794

Verginelli, I., Pecoraro, R., & Baciocchi, R. (2018). Using dynamic flux chambers to estimate the natural attenuation rates in the subsurface at petroleum contaminated sites. *Science of the Total Environment*, *619–620*, 470–479. https://doi.org/10.1016/j.scitotenv.2017.11.100

Wang, Y., Choi, Y., Zeng, T., Davis, D., Buhr, M., Gregory Huey, L., & Neff, W. (2007). Assessing the photochemical impact of snow NO_x emissions over Antarctica during ANTCI 2003. *Atmospheric Environment*, *41*(19), 3944–3958. https://doi.org/10.1016/j.atmosenv.2007.01.056

Werle, P., Mücke, R., & Slemr, F. (1993). The limits of signal averaging in atmospheric trace-gas monitoring by tunable diode-laser absorption spectroscopy (TDLAS). *Applied Physics B: Photophysics and Laser Chemistry*, *57*(2), 131–139. https://doi.org/10.1007/BF00425997

Winton, V. H. L., Ming, A., Caillon, N., Hauge, L., Jones, A. E., Savarino, J., et al. (2020). Deposition, recycling, and archival of nitrate stable isotopes between the air-snow interface: Comparison between Dronning Maud Land and Dome C, Antarctica. *Atmospheric Chemistry and Physics*, *20*(9), 5861–5885. https://doi.org/10.5194/acp-20-5861-2020

Zatko, M., Geng, L., Alexander, B., Sofen, E., & Klein, K. (2016). The impact of snow nitrate photolysis on boundary layer chemistry and the recycling and redistribution of reactive nitrogen across Antarctica and Greenland in a global chemical transport model. *Atmospheric Chemistry and Physics*, *16*(5), 2819–2842. https://doi.org/10.5194/acp-16-2819-2016

Zatko, M. C., Grenfell, T. C., Alexander, B., Doherty, S. J., Thomas, J. L., & Yang, X. (2013). The influence of snow grain size and impurities on the vertical profiles of actinic flux and associated NO_x emissions on the Antarctic and Greenland ice sheets. *Atmospheric Chemistry and Physics*, *13*(7), 3547–3567. https://doi.org/10.5194/acp-13-3547-2013

Zhu, C., Xiang, B., Chu, L. T., & Zhu, L. (2010). 308 nm photolysis of nitric acid in the gas phase, on aluminum surfaces, and on ice films. *The Journal of Physical Chemistry A*, *114*(7), 2561–2568. https://doi.org/10.1021/jp909867a

Zhu, C., Xiang, B., Zhu, L., & Cole, R. (2008). Determination of absorption cross sections of surface-adsorbed HNO_3 in the 290–330 nm region by Brewster angle cavity ring-down spectroscopy. *Chemical Physics Letters*, *458*(4–6), 373–377. https://doi.org/10.1016/j.cplett.2008.04.125